

Chemistry–A European Journal

Supporting Information

Organoiridium Complexes Enhance Cellular Defense Against Reactive Aldehydes Species

Rahul D. Jana, Anh H. Ngo, Sohini Bose, and Loi H. Do*

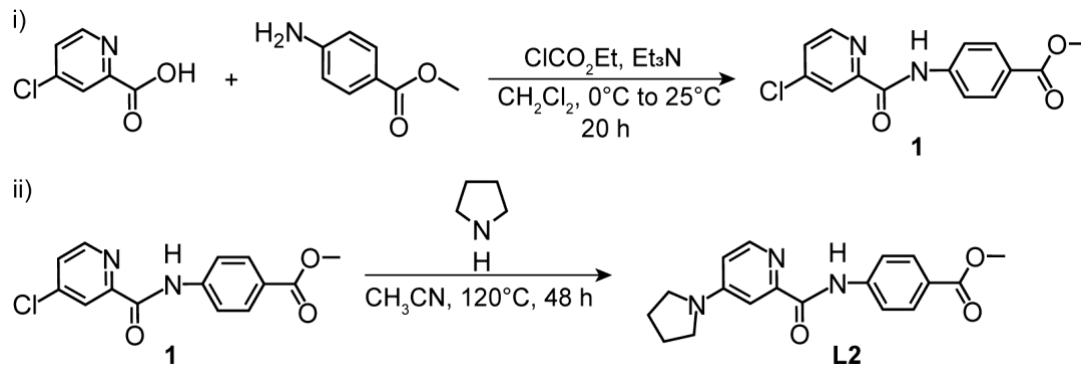
<u>Table of Contents</u>		<u>Page(s)</u>
Experimental Section		
Scheme S1	Synthesis of L2 and Ir2	S3
Scheme S2	Synthesis of 4-HNE and 4-ONE	S4
	Synthesis and Characterization	S5-S7
Experimental Data		
Figure S1	GC chromatogram of Transfer Hydrogenation Reactions	S7
Table S1	Transfer Hydrogenation of 4-HNE under Biologically Relevant Conditions	S8
Table S2	Transfer Hydrogenation with Low Concentrations of 4-HNE	S9
Figure S2	Transfer Hydrogenation of 4-ONE	S9
Figure S3	¹ H NMR Spectrum of 4-ONE Reduced Product	S10
Figure S4	Time-dependent ¹ H NMR Spectra of 4-HNE + Ir2 /HCOONa	S11
Figure S5	GC-mass Spectra of Isotope-labeled II in Different Reaction Conditions	S12
Figure S6	¹ H NMR Spectra of II , Formed from Reaction of 4-HNE with HCOONa/DCOONa by Ir2	S13
Scheme S3	Possible Mechanism of Transfer Hydrogenation of Catalyzed by Ir Complex	S14
Figure S7	Log <i>P</i> , IC ₅₀ and [Ir] of Ir Complexes in NIH-3T3	S14
Table S3	Accumulation of Iridium in NIH-3T3 cells (10 μM)	S15
Table S4	Accumulation of Iridium in NIH-3T3 cells (20 μM)	S16
Figure S8	Comparison of ICP-MS Results for Ir Complexes in NIH-3T3 cells	S17
Table S5	ICP-MS Results for Ir Complexes in SH-SY5Y cells	S18
Figure S9	Plot of Cell Viability (%) vs Iridium Concentration in NIH-3T3 cells	S19
Figure S10	Effect of reduced alcohol products on the cytotoxicity of Ir ₂ in NIH-3T3 cells	S20
Figure S11	IC ₅₀ of Iridium Complexes in NIH-3T3 cells	S21
Figure S12	Effect of HCOONa on the Cytotoxicity of Ir Complexes in NIH-3T3 cells	S22
Figure S13	IC ₅₀ of Aldehydes, Alcohols, and Aldehyde Scavengers in NIH-3T3 cells	S23
Figure S14	4-HNE Detoxification by Iridium Complexes in SH-SY5Y cells	S24
Figure S15	Detoxification of 4-HNE by Ir Complexes in NIH-3T3 cells	S25
Figure S16	Comparing 4-HNE Detoxification Ability of Iridium Complexes and Aldehyde Scavengers in NIH-3T3 cells	S26
Figure S17	Effects of GSH on 4-HNE detoxification by Ir2 in NIH-3T3 cells	S27
Figure S18	Detoxification of 4-ONE by Ir Complexes in SH-SY5Y cells	S28

Figure S19	Comparing 4-ONE Detoxification Ability of Iridium Complexes and Aldehyde Scavengers in SH-SY5Y cells	S29
Figure S20	4-ONE Detoxification by Iridium Complexes in NIH-3T3 cells	S30
Figure S21	4-HNE Detoxification by Ir Complexes in SH-SY5Y Cells with the Addition of 4-HNE for Three Consecutive Days	S31
Figure S22	Effect of Ir Concentration in 4-HNE Detoxification Inside SH-SY5Y Cells with the Addition of 4-HNE for Three Consecutive Days	S32
Figure S23	4-HNE Detoxification by Aldehyde Scavengers in SH-SY5Y Cells with the Addition of 4-HNE for Three Consecutive Days	S33
NMR Characterization Data		
Figures S24-S29	^1H and ^{13}C NMR of Ligand L2 and Ir2 Complex	S34-S39
Figures S30-S38	^1H and ^{13}C NMR of 4-HNE and 4-ONE, their Reduced Alcohol Products	S40-S48
References		S49

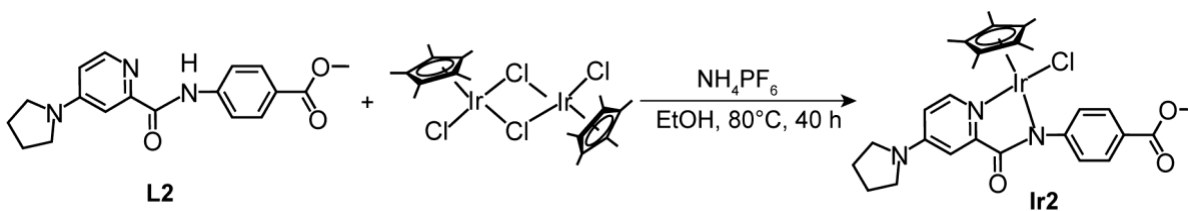
EXPERIMENTAL SECTION

Synthesis and Characterization

A. Synthesis of Ligand **L2**

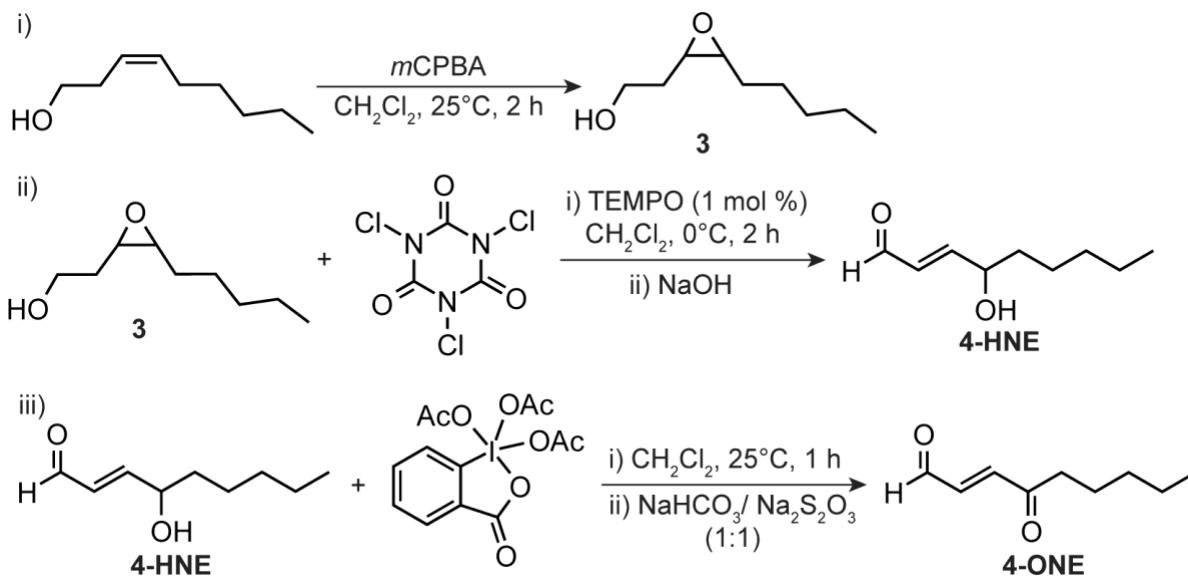


B. Synthesis of Complex **Ir2**

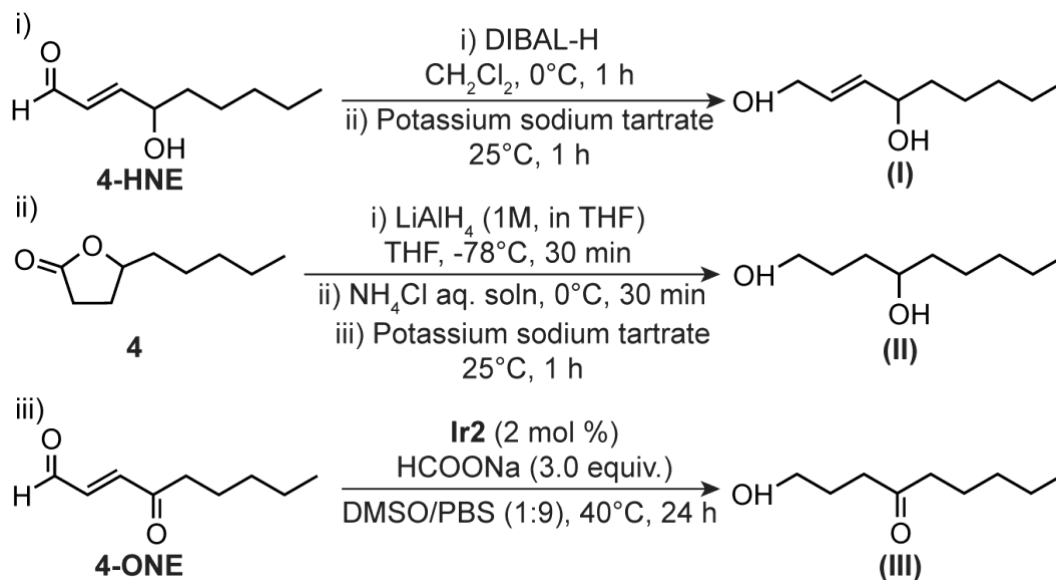


Scheme S1. Synthetic scheme for the preparation of ligand (**L2**, A) and its corresponding iridium complex (**Ir2**, B).

A. Synthesis of 4-hydroxynon-2-enal (4-HNE) and 4-oxonon-2-enal (4-ONE)

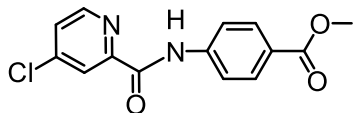


B. Synthesis of reduced alcohol products derived from 4-HNE and 4-ONE



Scheme S2. Synthetic scheme for the preparation of aldehydes 4-HNE and 4-ONE (A) and their reduced alcohol products (B).

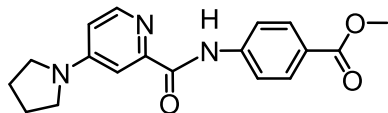
Preparation of Compound 1. In a 200 mL round bottom flask, 4-chloro-2-pyridinecarboxylic acid (1.58 g, 10.0 mmol, 1.0 equiv.) was dissolved in ~100 mL of anhydrous dichloromethane, and cooled in an ice bath



for ~15 min. Triethylamine (2.79 mL, 20.0 mmol, 2.0 equiv.) was added and stirred for 15 min. The mixture was then treated with ethyl chloroformate (1.24 mL, 13.0 mmol, 1.3 equiv.) and stirred in an ice bath for another 30 min before combining with methyl 4-aminobenzoate (0.91 g, 6.0 mmol, 0.6

equiv.). The reaction was stirred in an ice bath for 1 h, warmed to RT, and stirred for another 20 h. Once the reaction was complete, water was added and the organic phase was separated, dried over sodium sulfate, and evaporated to dryness. The crude product was purified by washing with diethyl ether, followed by recrystallization in dichloromethane to obtain a white solid (462 mg, 27% yield). ^1H NMR (CDCl_3 , 600 MHz): δ 10.10 (s, 1H), 8.53 (d, $J = 5.1$ Hz, 1H), 8.30 (d, $J = 2.0$ Hz, 1H), 8.08 (d, $J = 8.3$ Hz, 2H), 7.85 (d, $J = 8.3$ Hz, 2H), 7.51 (dd, $J = 4.9, 2.0$ Hz, 1H), 3.92 (s, 3H). $^{13}\text{C}\{^1\text{H}\}$ NMR (CDCl_3 , 126 MHz): δ 166.68, 161.10, 150.89, 149.04, 146.54, 141.58, 131.05, 127.07, 126.04, 123.29, 119.06, 52.18. GC-MS: calculated for $\text{C}_{14}\text{H}_{11}\text{ClN}_2\text{O}_3$ $m/z = 290.0$ $[\text{M}]^+$, found $m/z = 290.4$.

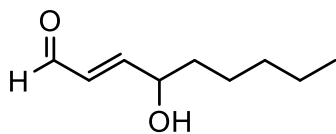
Preparation of Ligand L2. In a high-pressure glass tube, compound 1 (290.7 mg, 1.0 mmol, 1 equiv.) and pyrrolidine (1.7 mL, 20 mmol, 20 equiv.) were combined with 5.0 mL of acetonitrile in a high-pressure glass



tube. The tube was sealed tightly using a Teflon screw cap and the mixture was stirred at 120 °C for 48 h. After removing the solvent and unreacted pyrrolidine by high vacuum, the resulting off-white solid was washed with methanol (3x10 mL) to obtain a white solid (263 mg, 81%

yield). ^1H NMR (CDCl_3 , 600 MHz): δ 10.37 (s, 1H), 8.16 (d, $J = 5.7$ Hz, 1H), 8.06 (d, $J = 8.4$ Hz, 2H), 7.85 (d, $J = 8.5$ Hz, 2H), 7.40 (s, 1H), 6.48 (dd, $J = 6.1, 2.1$ Hz, 1H), 3.90 (s, 3H), 3.39 (s, 4H), 2.06 (m, 4H). $^{13}\text{C}\{^1\text{H}\}$ NMR (CDCl_3 , 126 MHz): 166.86, 163.53, 152.92, 149.41, 148.00, 142.31, 130.98, 125.34, 118.87, 109.02, 105.81, 52.11, 47.40, 25.46 ppm. GC-MS: calculated for $\text{C}_{18}\text{H}_{19}\text{N}_3\text{O}_3$ $m/z = 325.1$ $[\text{M}]^+$, found $m/z = 325.5$.

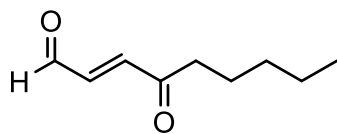
Preparation of 4-hydroxynon-2-enal (4-HNE). This synthetic method was modified from the procedure



described by Gardner et. al.¹ To a solution of compound 3 (344 mg, 2.18 mmol) in 30 mL of anhydrous CH_2Cl_2 at 0 °C, trichloroisocyanuric acid (TCICA) (535 mg, 2.29 mmol) was added slowly. The reaction mixture was stirred for 5 min at 0 °C. TEMPO was then added to the reaction mixture and

stirred for another 2 h at 0 °C. After the reaction was complete, 30 mL of water was added, and the mixture was stirred vigorously for 10 min to obtain a clear light-yellow solution. The organic layer was then washed with 1.0 M NaOH (3x20 mL). The organic extract was dried over sodium sulfate and evaporated to dryness to yield a light yellow oil (259 mg, 76%). This compound was stored at -20 °C to minimize decomposition. ^1H NMR (CDCl_3 , 400 MHz): δ 9.58 (d, $J = 7.7$ Hz, 1H), 6.82 (dd, $J = 15.8, 4.6$ Hz, 1H), 6.38-6.24 (m, 1H), 4.44 (q, $J = 6.5, 5.8$ Hz, 1H), 1.67-1.59 (m, 2H), 1.36-1.28 (m, 6H), 0.93-0.86 (m, 3H) ppm. ^{13}C NMR (CDCl_3 , 101 MHz): δ 194.23, 160.57, 130.12, 70.67, 36.11, 31.46, 24.78, 22.35, 13.85 ppm. The NMR spectra matched those reported previously.¹

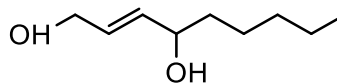
Preparation of 4-oxonon-2-enal (4-ONE).



This compound was synthesized according to a literature procedure with modification.² Solid Dess-Martin periodinane (156 mg, 1.0 mmol) was added slowly to a solution of 4-HNE in anhydrous CH₂Cl₂ (20 mL) and stirred at 25 °C for 1 h. The reaction mixture was then washed with an aqueous solution containing NaHCO₃ and Na₂S₂O₃ (1:1, 3x15 mL). The

organic phase was dried over sodium sulfate and evaporated to dryness to obtain a yellow oil (52 mg, 33% yield). The ¹H NMR data are consistent with that reported in the literature.² ¹H NMR (CDCl₃, 400 MHz): δ 9.78 (d, *J* = 7.0 Hz, 1H), 6.88 (d, *J* = 16.2 Hz, 1H), 6.83-6.73 (m, 1H), 2.69 (t, *J* = 7.3 Hz, 2H), 1.70-1.63 (m, 2H), 1.36-1.27 (m, 4H), 0.90 (t, *J* = 6.9 Hz, 3H) ppm. ¹³C NMR (CDCl₃, 151 MHz): δ 200.31, 193.58, 145.09, 137.46, 41.32, 31.37, 23.48, 22.54, 14.00 ppm. The NMR spectra matched those reported previously.²

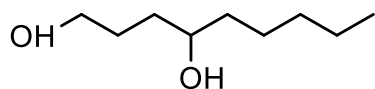
Preparation of non-2-ene-1,4-diol (I).



In a 50 mL round bottom flask, 4-HNE (136 mg, 0.87 mmol, 1.0 equiv.) was dissolved in 15 mL of anhydrous CH₂Cl₂ and cooled to 0 °C for 1 h. Diisobutylaluminium hydride (DIBAL-H, 1M in THF) (2.2 mL, 2.18 mmol, 2.5 equiv.) was added dropwise to the reaction mixture under an inert

atmosphere and stirred for 1 h at 0 °C. The reaction mixture was quenched with an aqueous solution of potassium sodium tartrate and stirred for another 3 h at RT. The aqueous layer was then extracted with CH₂Cl₂ (3x15 mL) and the combined organic fractions were dried over Na₂SO₄ and evaporated to a colorless oil (56 mg, 41 %). ¹H NMR (CDCl₃, 400 MHz): δ 5.79-5.73 (m, 1H), 5.70-5.63 (m, 1H), 4.11-4.04 (m, 3H), 3.34-3.08 (m, 2H), 1.53-1.41 (m, 2H), 1.35-1.22 (m, 6H), 0.86 (t, *J* = 6.3 Hz, 3H) ppm. ¹³C NMR (CDCl₃, 151 MHz): δ 134.63, 129.77, 72.38, 62.77, 37.19, 31.87, 25.22, 22.71, 14.14 ppm. The NMR spectra are consistent with those reported previously.³

Preparation of nonane-1,4-diol (II).



γ -Nonalactone (976 mg, 6.26 mmol, 1.0 equiv.) was dissolved in 20 mL of anhydrous THF and then cooled to -78 °C. A solution containing LiAlH₄ (1 M in THF, 13.2 mL, 13.14 mmol, 2.1 equiv.) was added dropwise to the reaction mixture under an inert atmosphere and stirred for 30 min

at -78 °C. The reaction flask was then warmed to 0 °C and an aqueous solution of saturated NH₄Cl was added dropwise, leading to the formation of H₂ gas and a thick white mixture. The reaction mixture was stirred for another 30 min at 0 °C, warmed to RT, and combined with a solution of potassium sodium tartrate (25 mL), and stirred for another 1 h at RT. The organic layer was separated, and the aqueous layer was extracted with ethyl acetate (2x20 mL). The combined organic fractions were dried over Na₂SO₄ and evaporated to afford a colorless oil (765 mg, 76%). ¹H NMR (CDCl₃, 500 MHz): δ 3.78-3.56 (m, 3H), 2.48 (s, 2H), 1.78-1.58 (m, 2H), 1.48-1.45 (m, 4H), 1.35-1.24 (m, 6H), 0.88 (t, *J* = 6.7 Hz, 3H) ppm. ¹³C NMR (CDCl₃, 101 MHz): δ 72.05, 63.15, 37.70, 34.53, 32.00, 29.27, 25.56, 22.78, 14.19 ppm. The NMR spectra are consistent with those reported previously.⁴

Preparation of 1-hydroxynonan-4-one (III). In a 20 mL vial, a mixture of 4-ONE (45 mg, 0.29 mmol, 1.0 equiv.), HCOONa (62 mg, 0.90 mmol, 3.0 equiv.), and iridium catalyst **Ir2** (4.1 mg, 0.006 mmol, 2 mol%) in DMSO:PBS (10:90) was heated at 40 °C for 24 h. Once the reaction was complete, the reaction mixture was extracted into diethyl ether (2x10 mL), concentrated, and then purified in silica gel column chromatography (15% EtOAc in hexane). Yield: 14 mg (30%). ¹H NMR (CDCl₃, 500 MHz): δ 3.68-3.64 (m, 2H), 2.58-2.54 (m, 2H), 2.45-2.38 (m, 2H), 1.87-1.80 (m, 2H), 1.33-1.26 (m, 6H), 0.89 (t, *J* = 7.0, 3H) ppm. The ¹H NMR spectrum is consistent with that reported previously.⁵

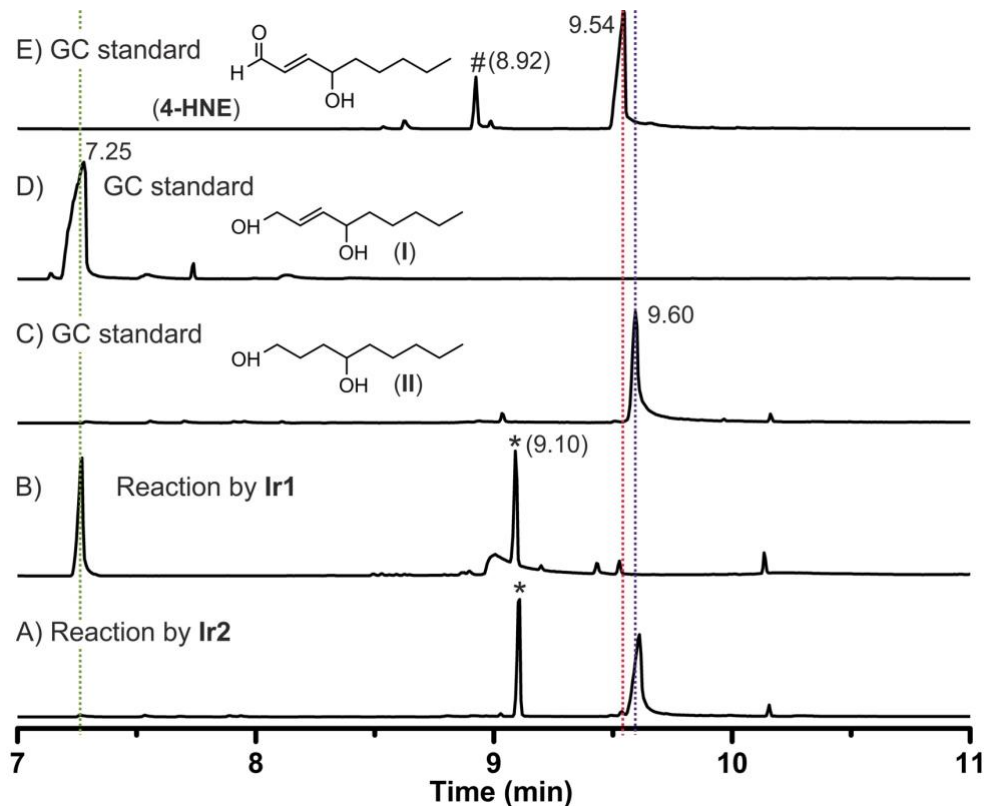
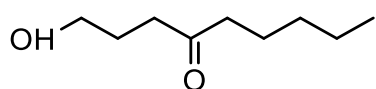
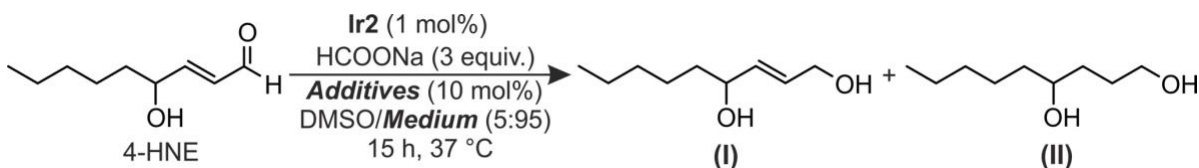


Figure S1. Gas chromatograms obtained from the reaction of 4-HNE (50 μmol) with HCOONa (150 μmol) and either A) **Ir1** or B) **Ir2** (0.50 μmol) in a mixture of DMSO/ PBS (5:95; 3 mL) at 37 °C for 15 h. GC traces of authentic samples of **II** (C), **I** (D), and **4-HNE** (E) for comparison. The peaks marked with an asterisk (*) indicate the presence of the internal standard pentamethylbenzene. The peak marked with a hastag (#) is assigned as a decomposition product of 4-HNE.

Table S1. Reduction of 4-HNE Using Ir2 and HCOONa Under Biologically Relevant Conditions^a

Entry	Media	Additives (equiv., relative to Ir)	Conversion (%)	Yield of I (%) ^b	Yield of II (%) ^b
1	PBS	-	97 ± 2	<1	94 ± 2
2 ^c	PBS	-	94	85	7
3 ^d	PBS	-	86 ± 2	30 ± 2	58 ± 2
4	RMPI-1640	-	97 ± 3	3 ± 1	88 ± 3
5	DMEM	-	98 ± 2	2 ± 1	93 ± 4
6	DMEM+ 10% FBS + 1% Penicillin Streptomycin	-	77 ± 2	58 ± 6	7 ± 3
7	DMEM	L-Glutathione reduced (10)	40 ± 2	26 ± 2	11 ± 2
8	DMEM	L-Glutathione reduced (20)	10 ± 2	3 ± 2	0
9	DMEM	L-Cysteine (10)	7 ± 2	3 ± 2	0
10	DMEM	L-Histidine (10)	95 ± 2	14 ± 1	83 ± 2
11	DMEM	L-Lysine (10)	96 ± 1	3 ± 2	86 ± 2

^aReaction conditions: 4-HNE (50 μmol), HCOONa (150 μmol), Ir complex (0.50 μmol), DMSO/Medium (5:95, 3 mL), 37 °C, 15 h. ^bThe reaction yields were quantified using gas chromatography with pentamethylbenzene as an internal standard. The yields shown are the average values obtained from triplicate runs. ^cThis reaction was carried out using Ir1 (1 mol %) instead of Ir2. ^dThe reaction was performed using NADH (150 μmol) instead of HCOONa as a hydride source.

Table S2. Reduction of 4-HNE Using Ir2 and HCOONa in DMEM^a

Entry	Concentration of 4-HNE (mM)	Ir2 loading (mol%)	Conversion (%)	Yield of I (%) ^b	Yield of II (%) ^b
1	17	170 μ M (1)	97 \pm 2	< 1	94 \pm 3
2	1.0	10 μ M (1)	26 \pm 3	21 \pm 2	0
3	0.5	10 μ M (2)	31 \pm 3	26 \pm 2	0
4	0.25	10 μ M (4)	38 \pm 3	33 \pm 4	3 \pm 2
5	0.25	50 μ M (20)	95 \pm 2	2.5 \pm 1	88 \pm 3

^aReaction conditions: HCOONa (5 mM), DMSO/DMEM (5:95, 3 mL), 37 °C, 15 h. ^bThe reaction yields were determined by gas chromatography using pentamethylbenzene as an internal standard. Yields are the average of triplicate runs.

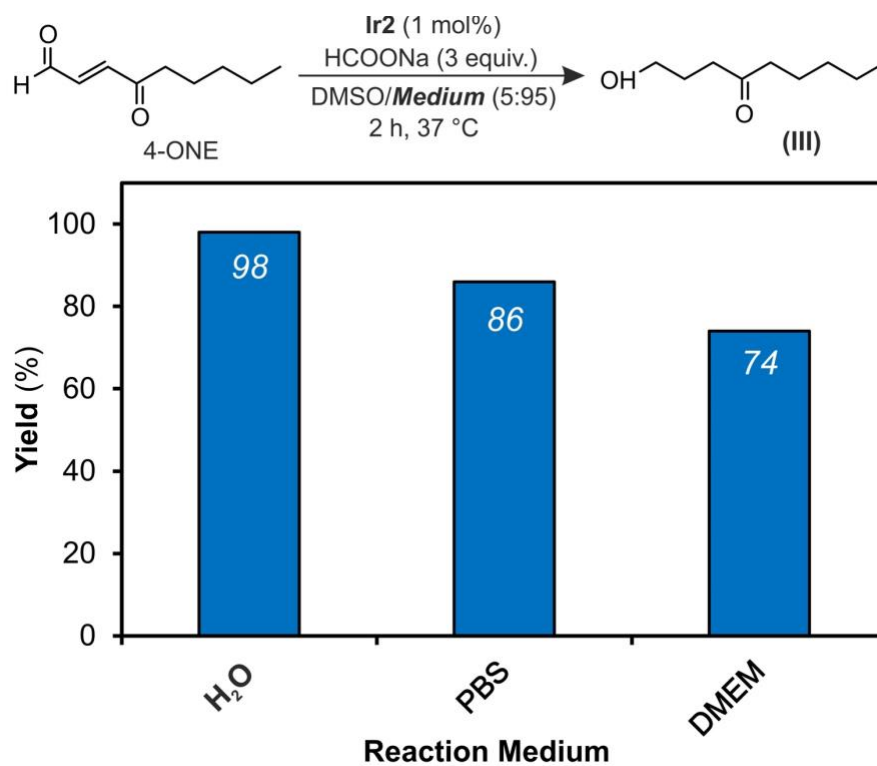


Figure S2. Transfer hydrogenation between 4-ONE and HCOONa catalyzed by Ir2 in biologically relevant media. Reaction conditions: 4-ONE (50 μ mol), HCOONa (150 μ mol), Ir2 (0.50 μ mol), DMSO/Medium (5:95, 3 mL), 37 °C, 2 h. The reaction yields were quantified by ¹H NMR spectroscopy using 1,3,5-trimethoxybenzene as an internal standard.

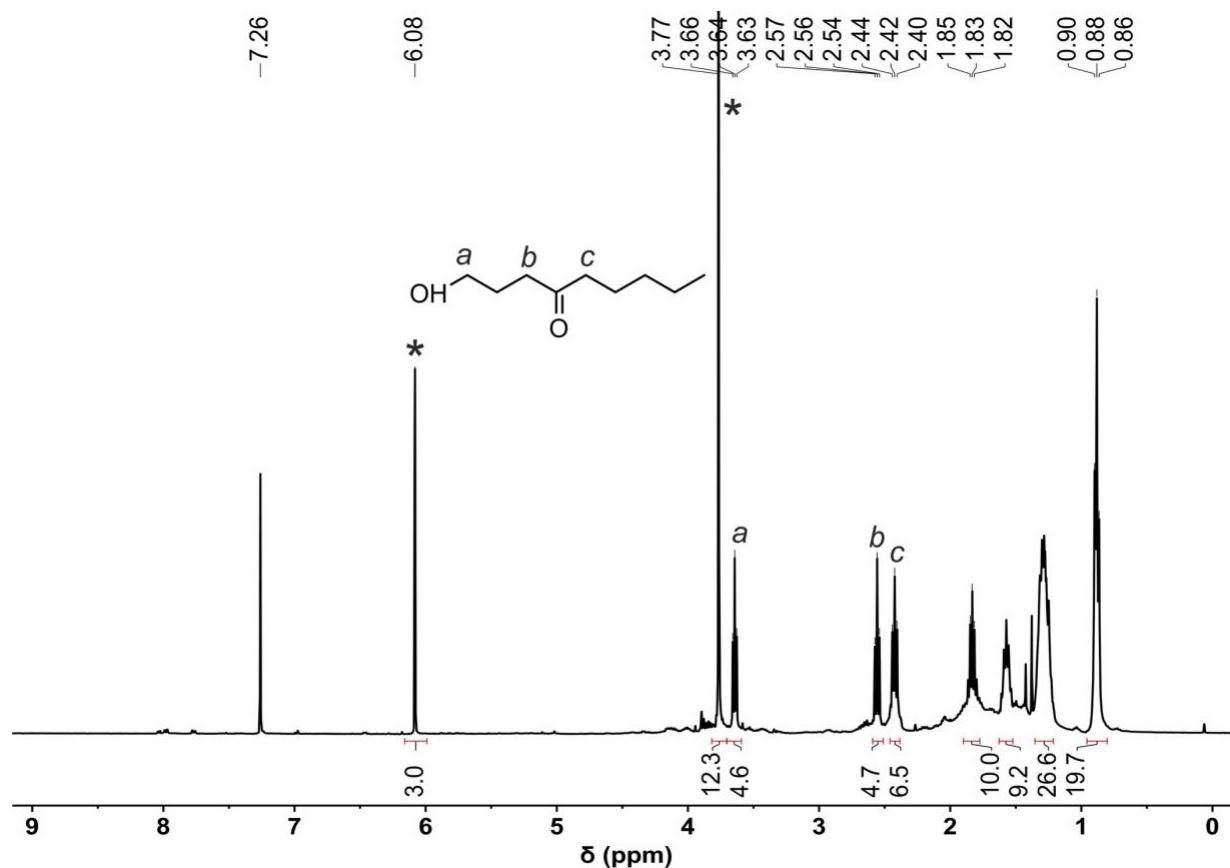


Figure S3. ^1H NMR (400 MHz, CDCl_3) spectrum of product **III** formed in the reaction of 4-ONE (50 μmol) with **Ir2** (0.50 μmol) and HCOONa (150 μmol) in DMEM at 37 $^\circ\text{C}$ for 2 h. The NMR peaks at 3.64, 2.56, and 2.42 ppm are consistent with those assigned to **III** in the literature.⁵ The peaks marked with an asterisk (*) correspond to the internal standard 1,3,5-trimethoxybenzene.

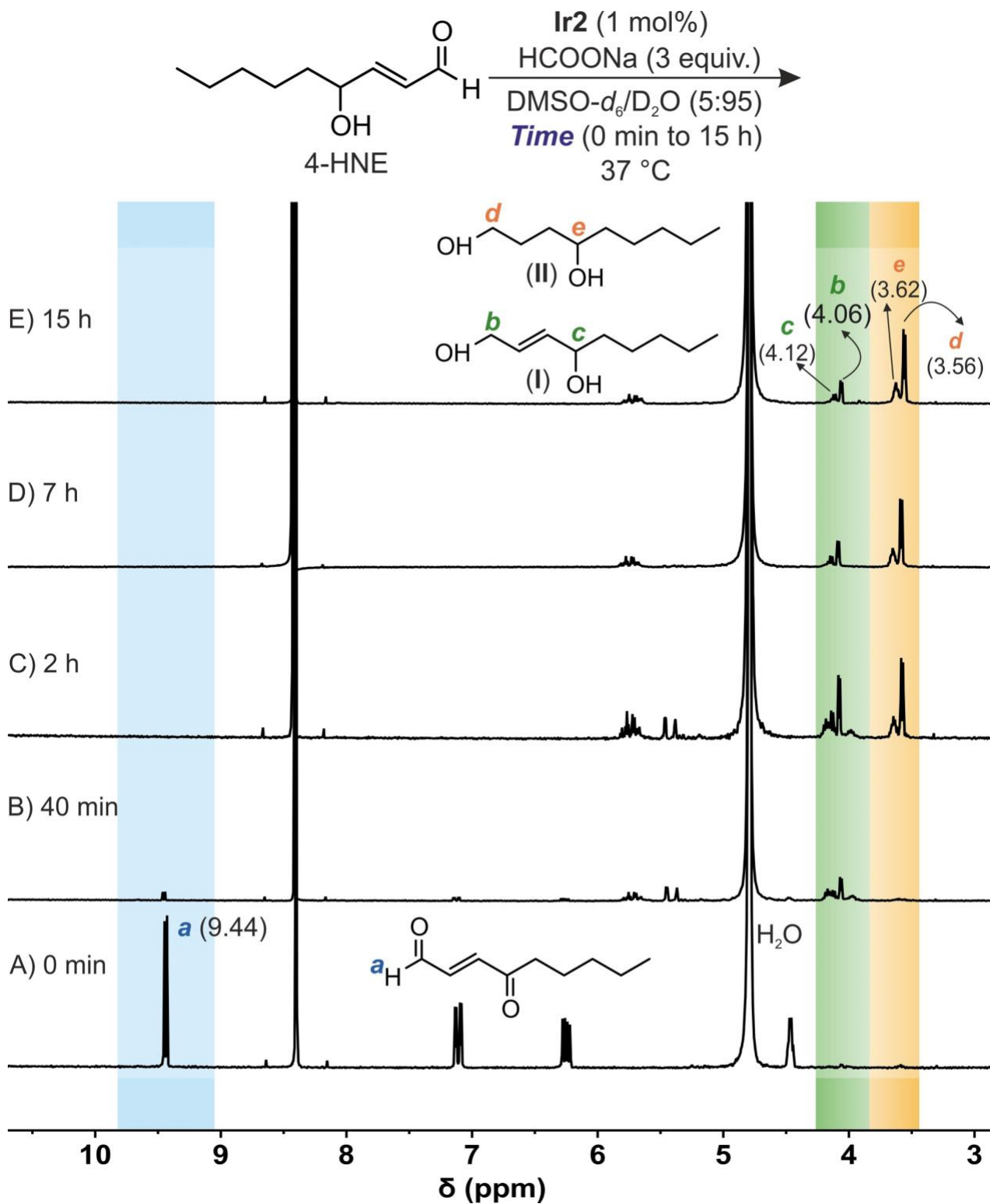


Figure S4. Time-dependent ^1H NMR spectra (400 MHz) obtained from the reaction of 4-HNE (50 μmol) with HCOONa (150 μmol) and **Ir2** complex (0.50 μmol) in a mixture of $\text{D}_2\text{O}/\text{DMSO-}d_6$ (95:5; 3 mL) at 37 °C. The peak assignments for 4-HNE (blue), **I** (green), and **II** (orange) are shown above in different colors.

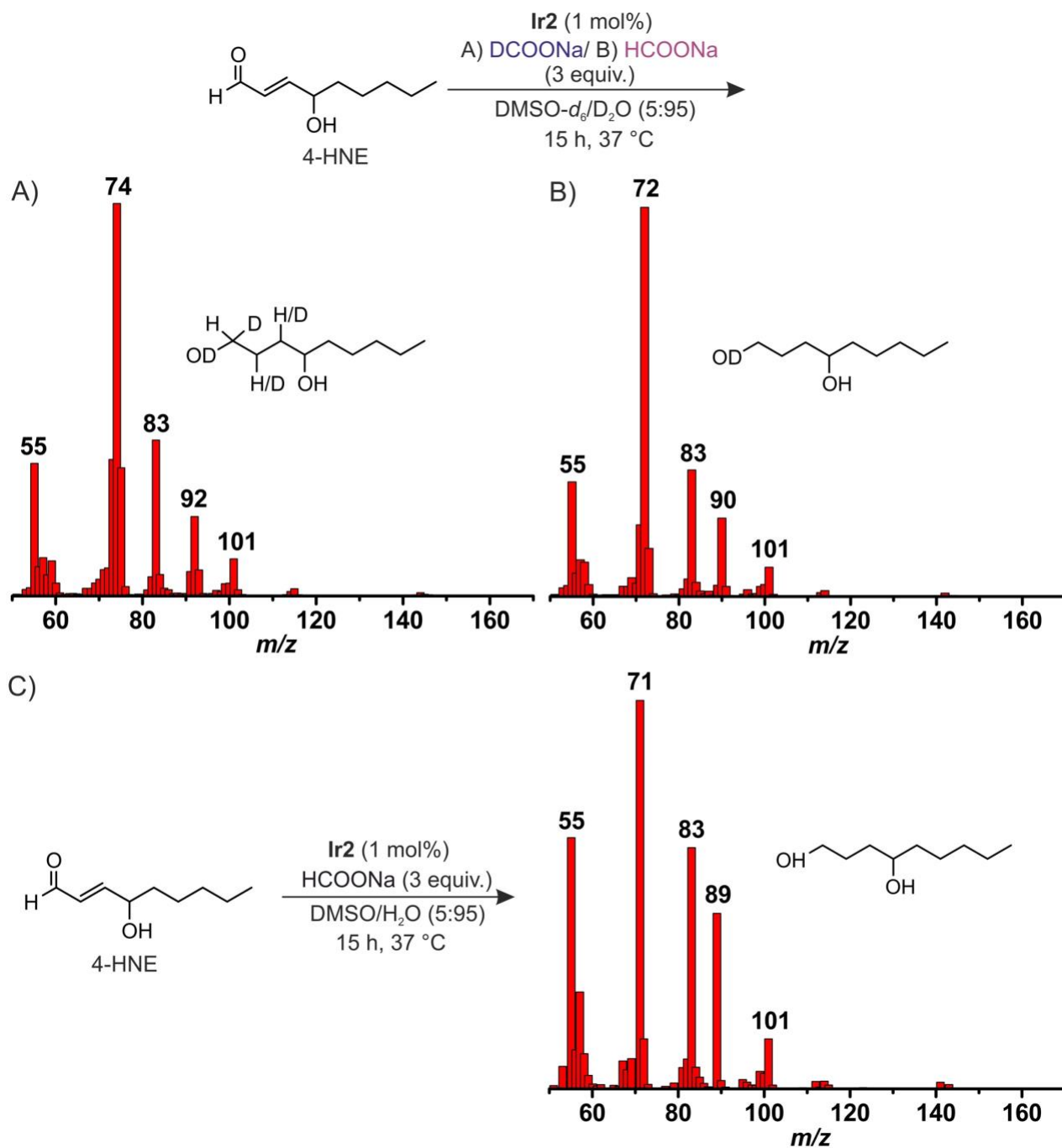


Figure S5. GC-mass spectra of nonane-1,4-diol (**I**) formed from the reaction of 4-HNE with A) DCOONa and B) HCOONa by **Ir2** complex in D₂O/DMSO-*d*₆ (95:5). C) GC-mass spectrum of isolated nonane-1,4-diol (**I**) formed in the reaction of 4-HNE with HCOONa and **Ir2** in H₂O/DMSO (95:5). The ion fragments of **I** in part C appear at *m/z* 71 for [M-(C₅H₁₃O)], and 89 for [M-(C₅H₁₁)], which are shifted to one or three mass units depending on the reaction conditions. The molecule ions parent [M]⁺ were not observed.

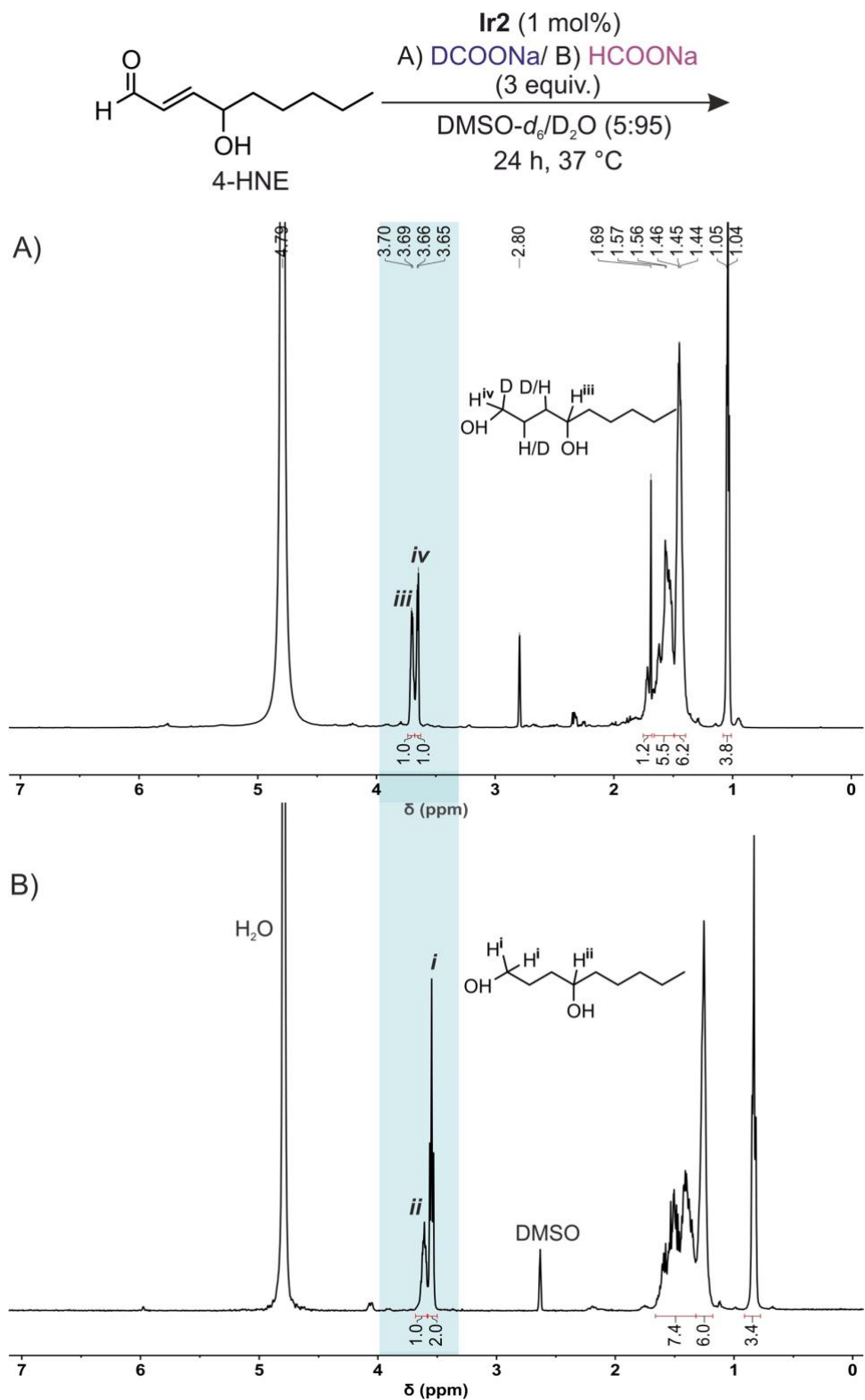
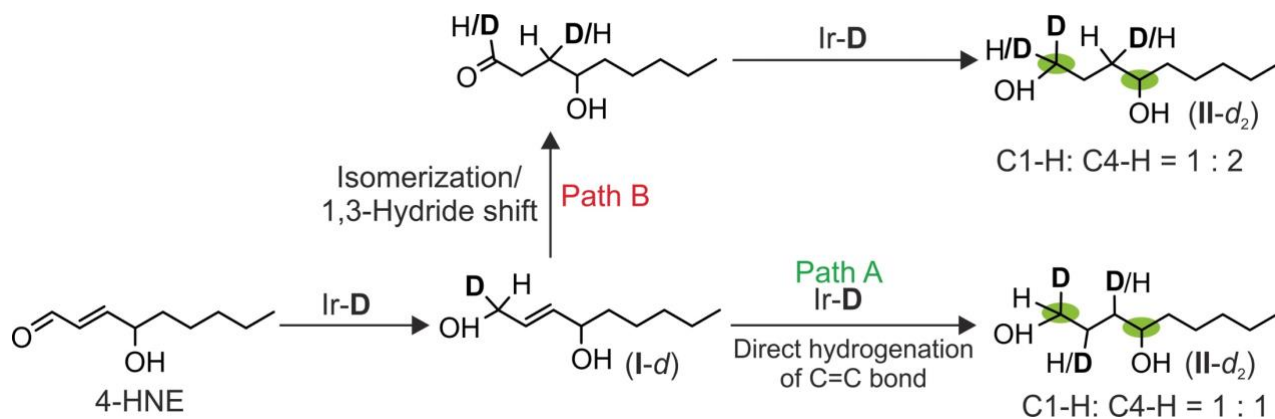


Figure S6. ¹H NMR spectra (400 MHz) spectra of compound **I** formed in the reaction of 4-HNE with HCOONa (A) or DCOONa (B) and **Ir2** in D₂O/DMSO-*d*₆ (95:5). Reaction conditions used: 4-HNE (50 μmol), HCOONa or DCOONa (150 μmol), Ir complex (0.50 μmol), D₂O/DMSO-*d*₆ (95:5; 3 mL), 37 °C, 15 h.



Scheme S3. Possible mechanisms for the transfer hydrogenation between 4-HNE and DCOONa catalyzed by Ir2 in H₂O. The ¹H NMR peak integration ratio between C1 and C4 is 1:1 in path A but is expected to be 1:2 in path B.

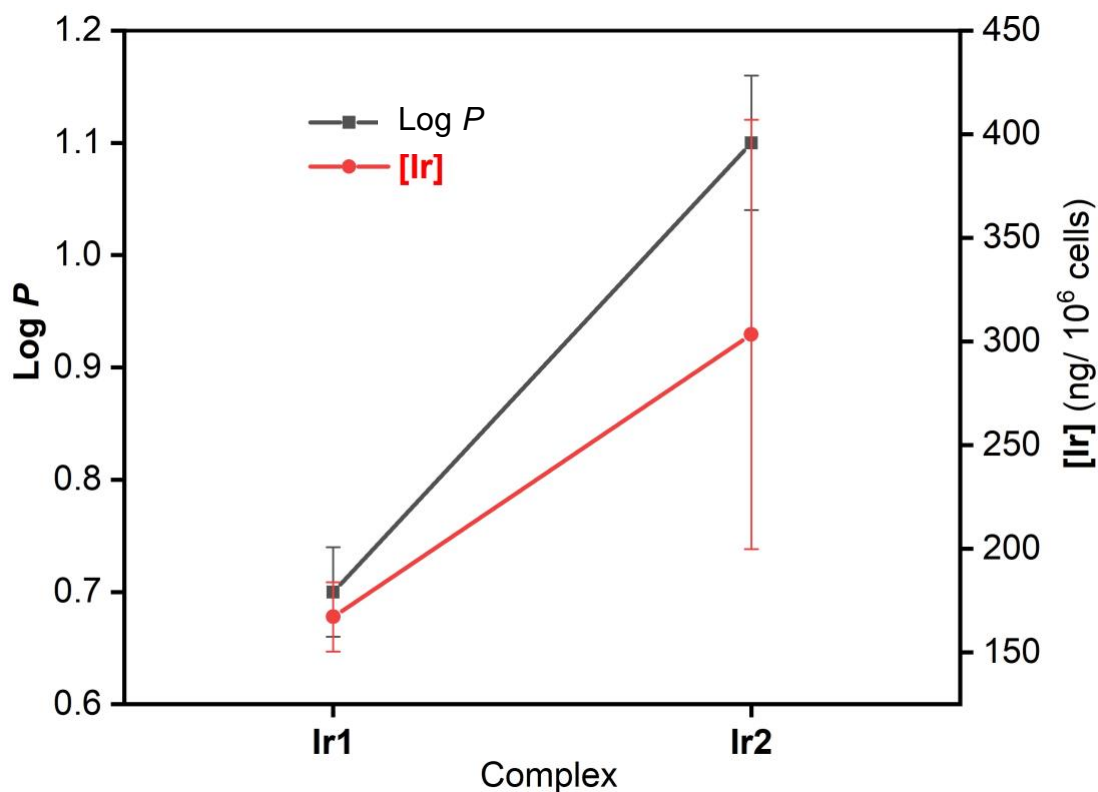


Figure S7. Comparison of the Log *P*, IC₅₀, and [Ir] of the iridium complexes in NIH-3T3 cells. The Log *P* values were calculated using the formula $[\text{Ir}]_{\text{octanol}}/[\text{Ir}]_{\text{water}}$, where $[\text{Ir}]_{\text{octanol}}$ is the concentration of the Ir complex in octanol and $[\text{Ir}]_{\text{water}}$ is the concentration of the Ir complex in water determined from the shake flask method. The IC₅₀ values are the half maximal inhibition concentration of NIH-3T3 cells after incubation with the Ir complexes for 3 h. The iridium accumulation inside NIH-3T3 cells (10 μM of Ir complexes and 3 h incubation) was measured using ICP-MS.

Table S3. Accumulation of Iridium Complexes in NIH-3T3 Cells^a

Time (h)	Complex	[Ir] (ppb)	Total Ir (ng)	Total Cells (x 10 ⁶)	[Ir] (ng/10 ⁶ cells)	Average [Ir] (ng/10 ⁶ cells)	Std. Dev.
Control		0.0	0.3	0.306	1.1	2.9	1.7
		0.2	1.5	0.286	5.1		
		0.1	0.7	0.288	2.4		
24	Ir1	4.9	34.5	0.185	186.7	197.7	11.0
		4.0	28.3	0.136	208.6		
		3.2	22.5	0.129	175.1		
		3.0	20.8	0.107	194.3		
	Ir2	3.3	23.2	0.055	422.4	341.1	81.4
		1.3	8.9	0.034	259.7		
		6.3	43.9	0.173	254.1		
		2.8	19.6	0.082	239.4		
3	Ir1	2.4	16.6	0.087	190.1	167.2	16.7
		1.1	8.0	0.050	160.5		
		1.0	7.0	0.047	150.9		
		0.6	4.0	0.038	105.3		
		0.6	4.2	0.033	127.3		
	Ir2	4.0	27.9	0.127	220.0	303.3	103.6
		3.0	21.0	0.047	449.3		
		1.6	11.3	0.047	240.6		
		2.0	14.1	0.086	163.0		
		2.7	18.7	0.081	230.6		

^aCells were incubated with 10 μ M of the Ir complexes.

Table S4 Accumulation of Iridium Complexes in NIH-3T3 Cells^a

Time (h)	Complex	[Ir] (ppb)	Total Ir (ng)	Total Cells (x 10⁶)	[Ir] (ng/10⁶ cells)	Average [Ir] (ng/10⁶ cells)	Std. Dev.
24	Ir1	25.4	178.1	0.183	971.4	858.0	103.3
		20.2	141.6	0.161	881.1		
		8.8	61.8	0.086	721.4		
	Ir2	13.0	91.1	0.049	1860.8	1380.3	340.7
		5.9	41.5	0.037	1110.1		
		6.6	45.9	0.039	1169.9		
3	Ir1	7.1	50.0	0.108	463.0	465.3	172.7
		10.5	73.7	0.109	677.9		
		1.1	8.0	0.031	255.0		
	Ir2	9.4	65.9	0.073	905.4	917.7	224.2
		8.8	61.8	0.052	1198.3		
		10.8	75.8	0.117	649.5		

^aCells were incubated with 20 μ M of the Ir complexes.

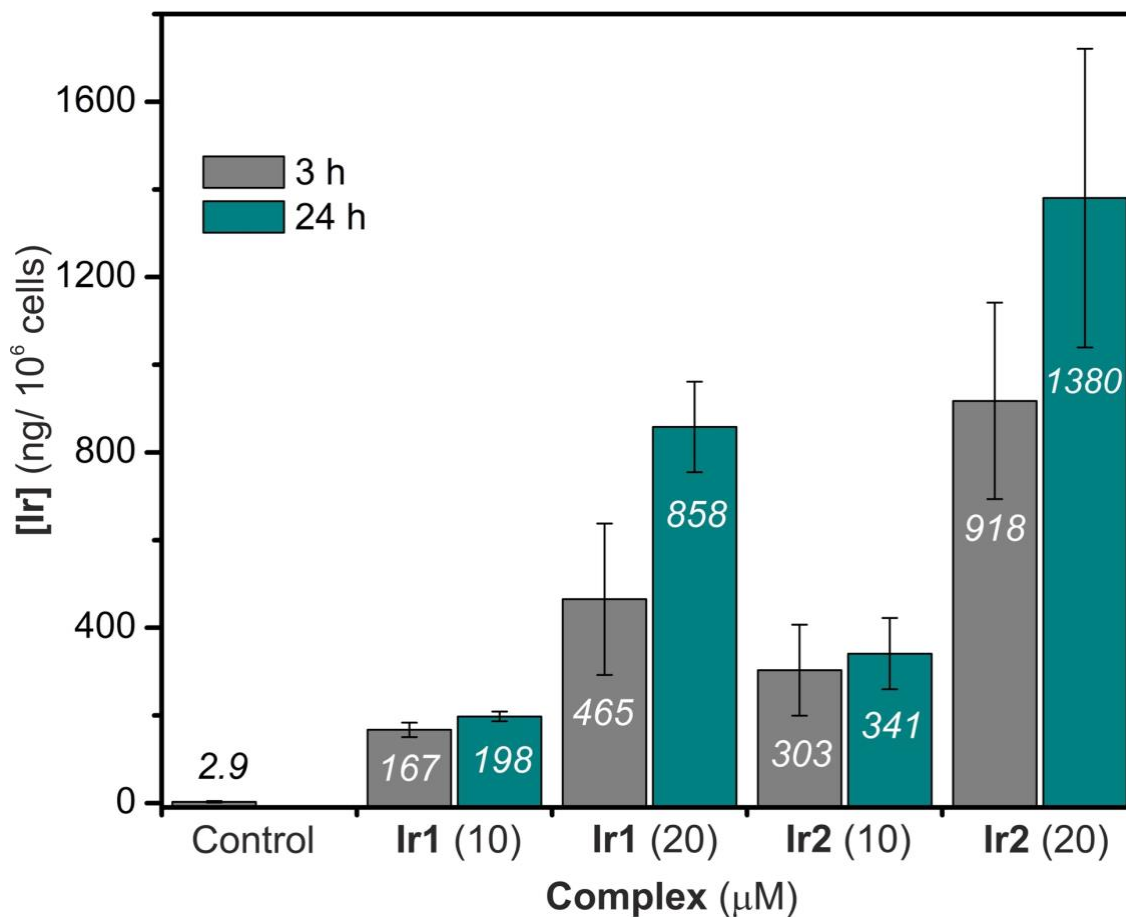


Figure S8. Comparing the effects of incubation time and concentration of the iridium complexes on their accumulation inside NIH-3T3 cells.

Table S5 Accumulation of Iridium Complexes in SH-SY5Y cells^a

Time (h)	Complex	[Ir] (ppb)	Total Ir (ng)	Total Cells (x 10 ⁶)	[Ir] (ng/10 ⁶ cells)	Average [Ir] (ng/10 ⁶ cells)	Std. Dev.
Control		0.004	0.031	0.1680	0.18	0.23	0.05
		0.004	0.030	0.1067	0.28		
24	Ir1	2.957	20.698	0.1177	175.90	168.6	39.2
		1.328	9.295	0.0793	117.27		
		2.004	14.027	0.0660	212.52		
		3.520	24.641	0.1105	223.07		
	Ir2	10.364	72.548	0.1667	435.29	488.8	53.5
		10.820	75.740	0.1397	542.29		
		1.655	11.585	0.0462	250.58		
		2.481	17.366	0.0827	210.07		
3	Ir1	1.473	10.311	0.0839	122.90	147.9	25.1
		5.457	38.199	0.2208	173.00		
		1.486	10.399	0.0787	132.08		
	Ir2	2.738	19.166	0.1203	159.27	258.3	99.0
		10.670	74.690	0.2090	357.37		
		1.636	11.452	0.0962	119.04		

^aCells were incubated with 5 μ M of the Ir complexes.

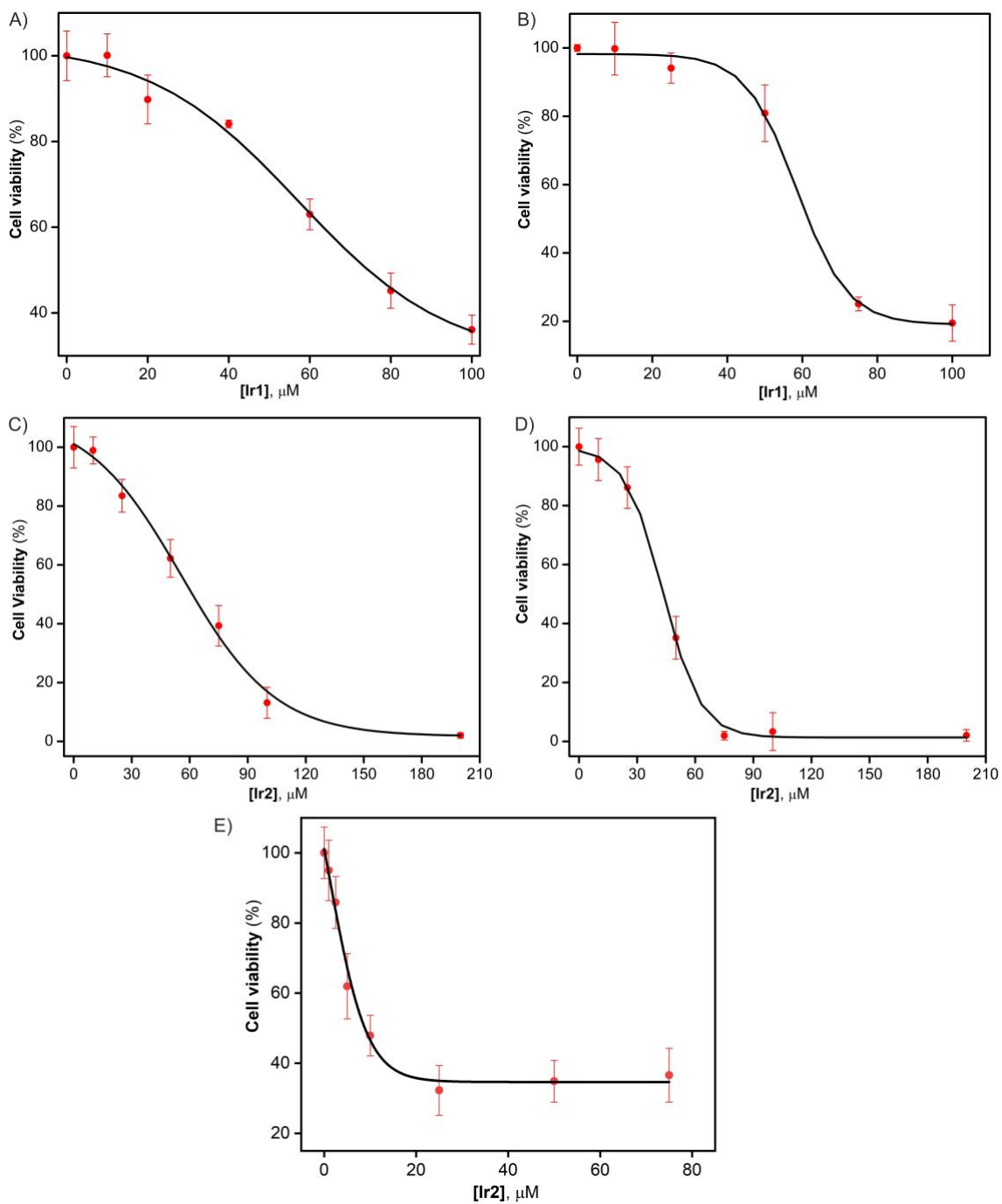


Figure S9. Cell viability curves obtained from incubation of NIH-3T3 cells with the iridium complexes. Treatment with A) **Ir1** for 3 h; B) **Ir1** for 24 h; C) **Ir2** for 3 h; D) **Ir2** for 24 h; and E) **Ir2** + GSH (100 μM) for 24 h.

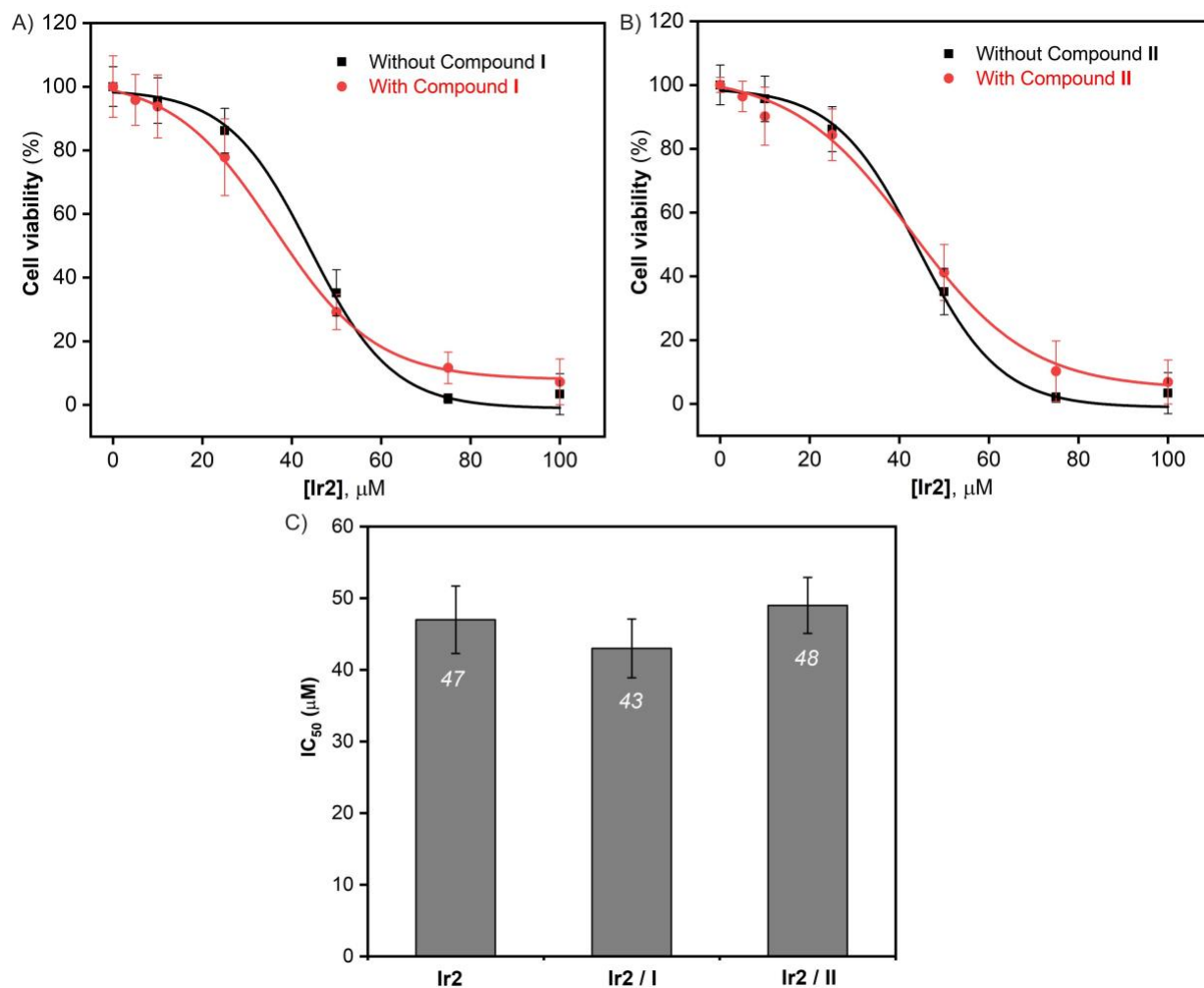
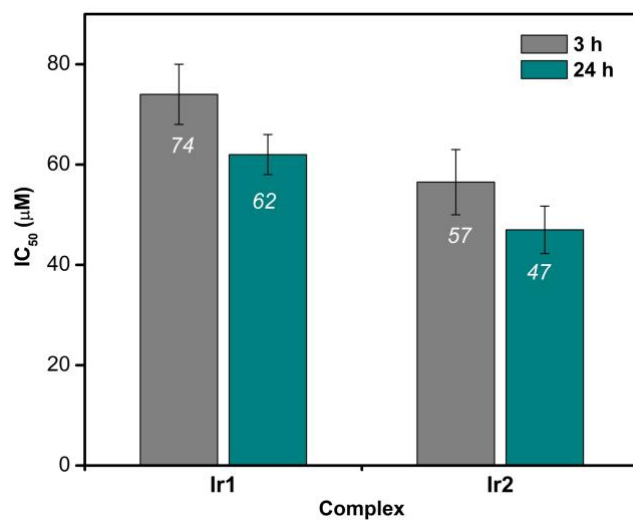


Figure S10. Cell viability curve obtained after incubating NIH-3T3 cells with A) **Ir2** ± **I** and B) **Ir2** ± **II** for 24 h. C) Comparison of the IC₅₀ values of **Ir2** in the presence and absence of **I** and **II** (100 μM) in NIH-3T3 cells (incubation time: 24 h).

A) NIH-3T3



B) NIH-3T3 vs. SH-SY5Y

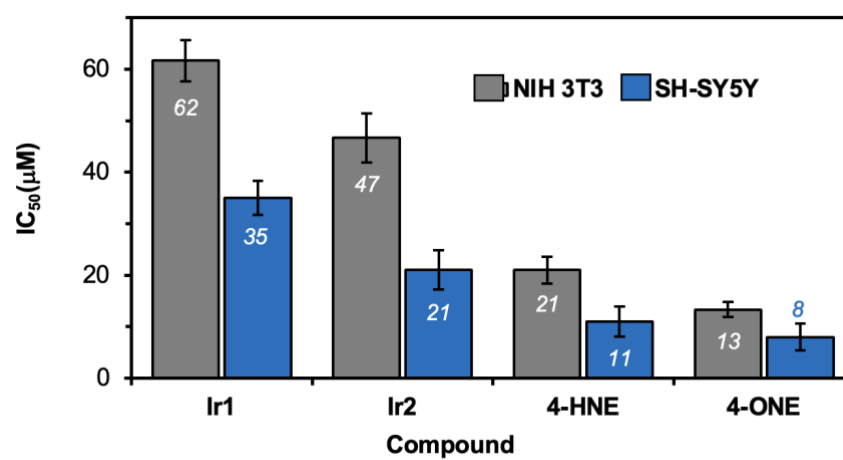


Figure S11. Comparing the IC₅₀ values in A) NIH-3T3 cells after treatment for 3 and 24 h; and B) NIH-3T3 vs. SH-SY5Y cells after treatment for 24 h.

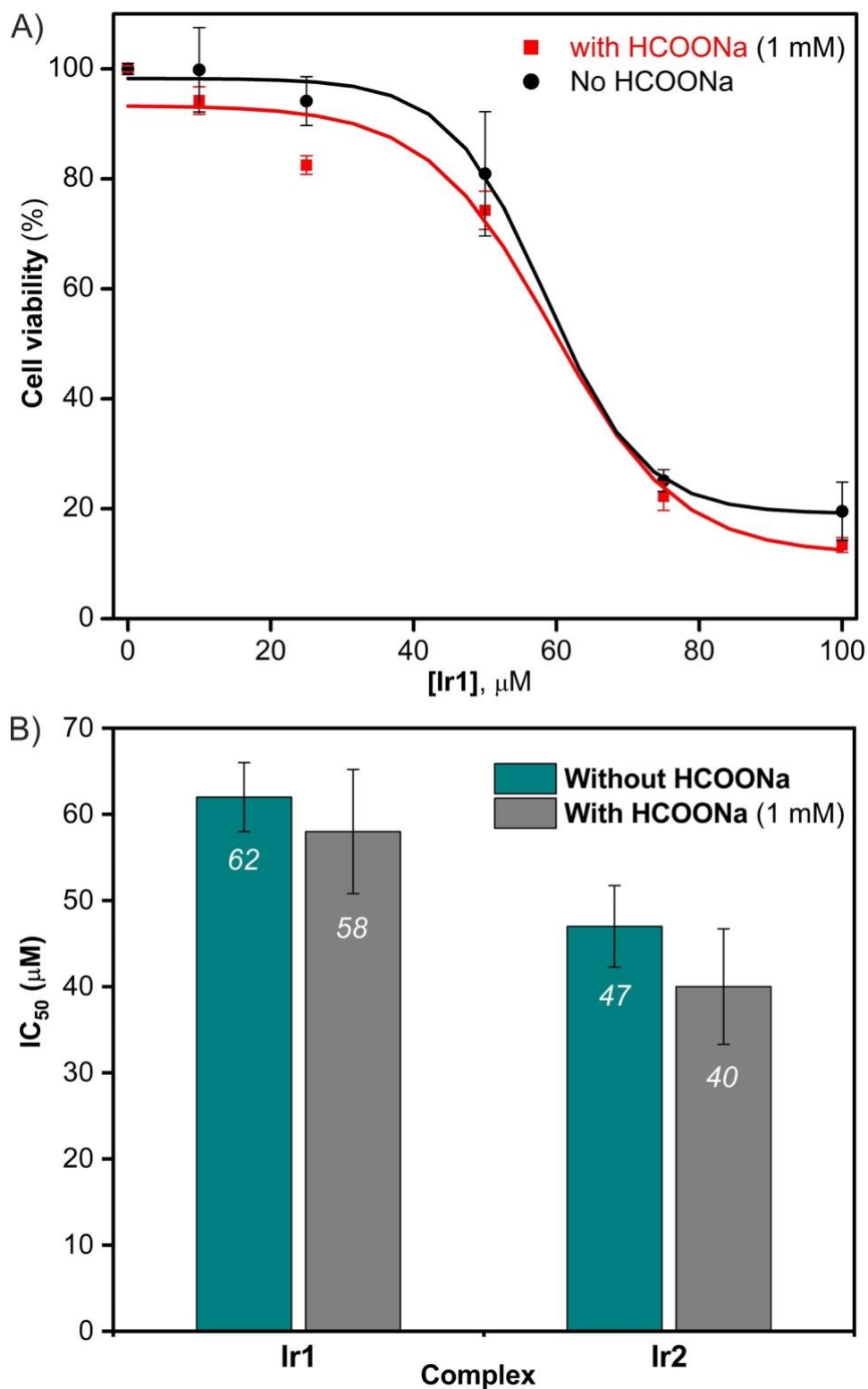


Figure S12. A) Cell viability curve obtained after incubating NIH-3T3 cells with Ir1 \pm HCOONa for 24 h. B) Comparison of the IC₅₀ values of iridium complexes in the presence and absence of HCOONa (1mM) in NIH-3T3 cells (incubation time: 24 h).

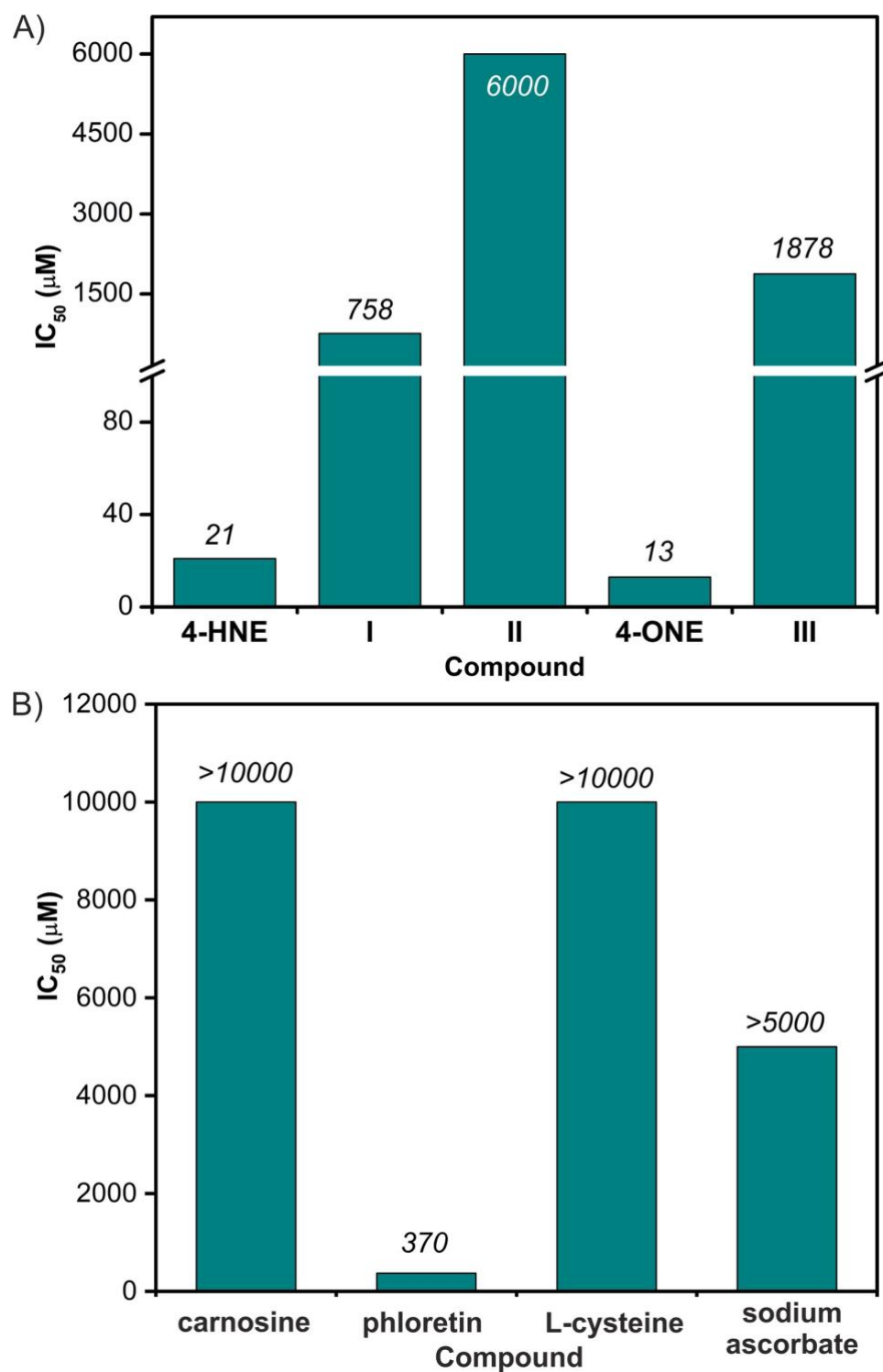


Figure S13. Comparison of the IC₅₀ values (24 h incubation) of aldehydes, alcohol, and aldehyde scavengers in NIH-3T3 cells: A) Aldehydes 4-HNE and 4-ONE and alcohols I, II, and III; B) aldehyde scavengers carnosine, phloretin, L-cysteine, and sodium ascorbate.

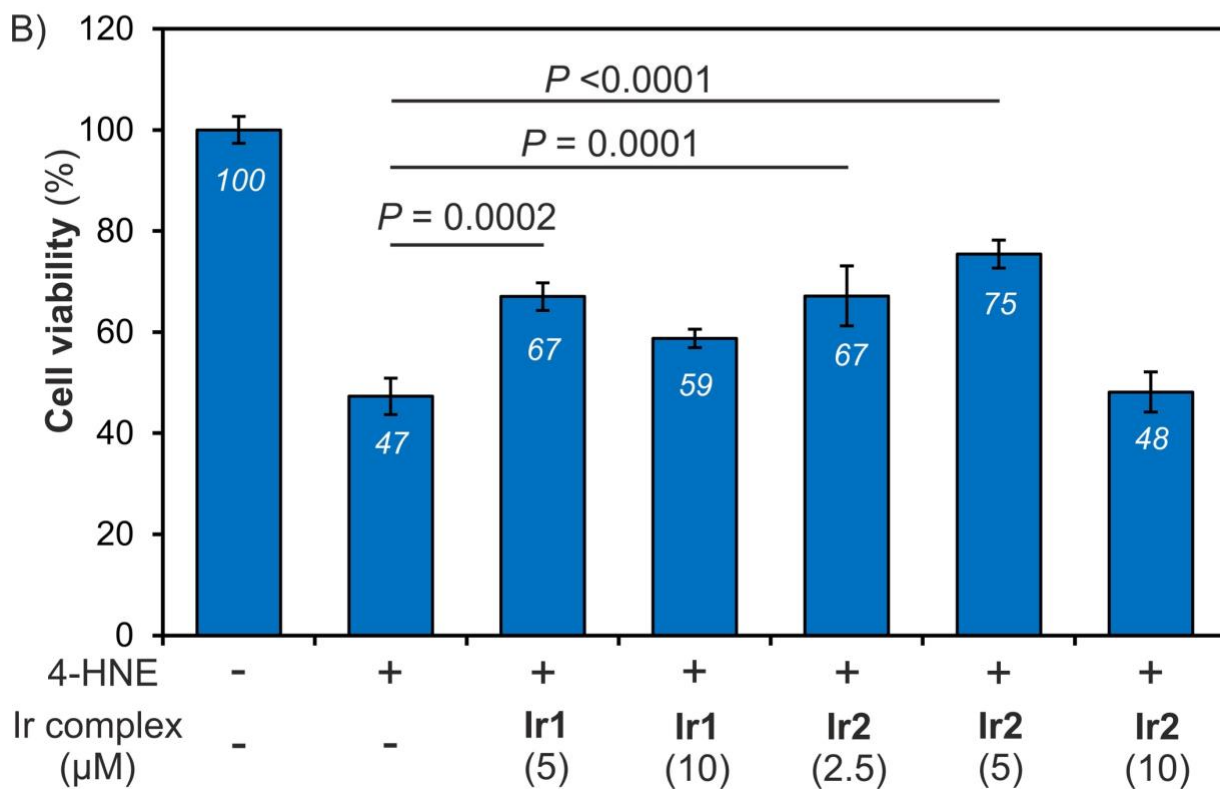
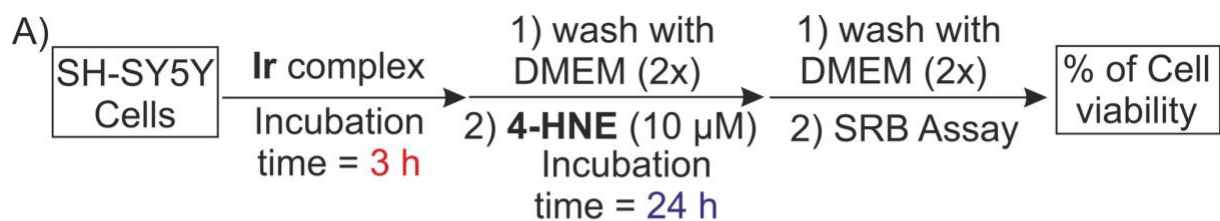


Figure S14. A) Experimental procedure for 4-HNE detoxification in SH-SY5Y cells. B) Effect of iridium complexes on SH-SY5Y cell viability in the presence of 4-HNE (10 μM). Treatment conditions: Ir complex (2.5, 5, or 10 μM), and 4-HNE (10 μM). The data were analyzed using one-way ANOVA and shown as the mean ± standard deviation ($n = 6$ per group).

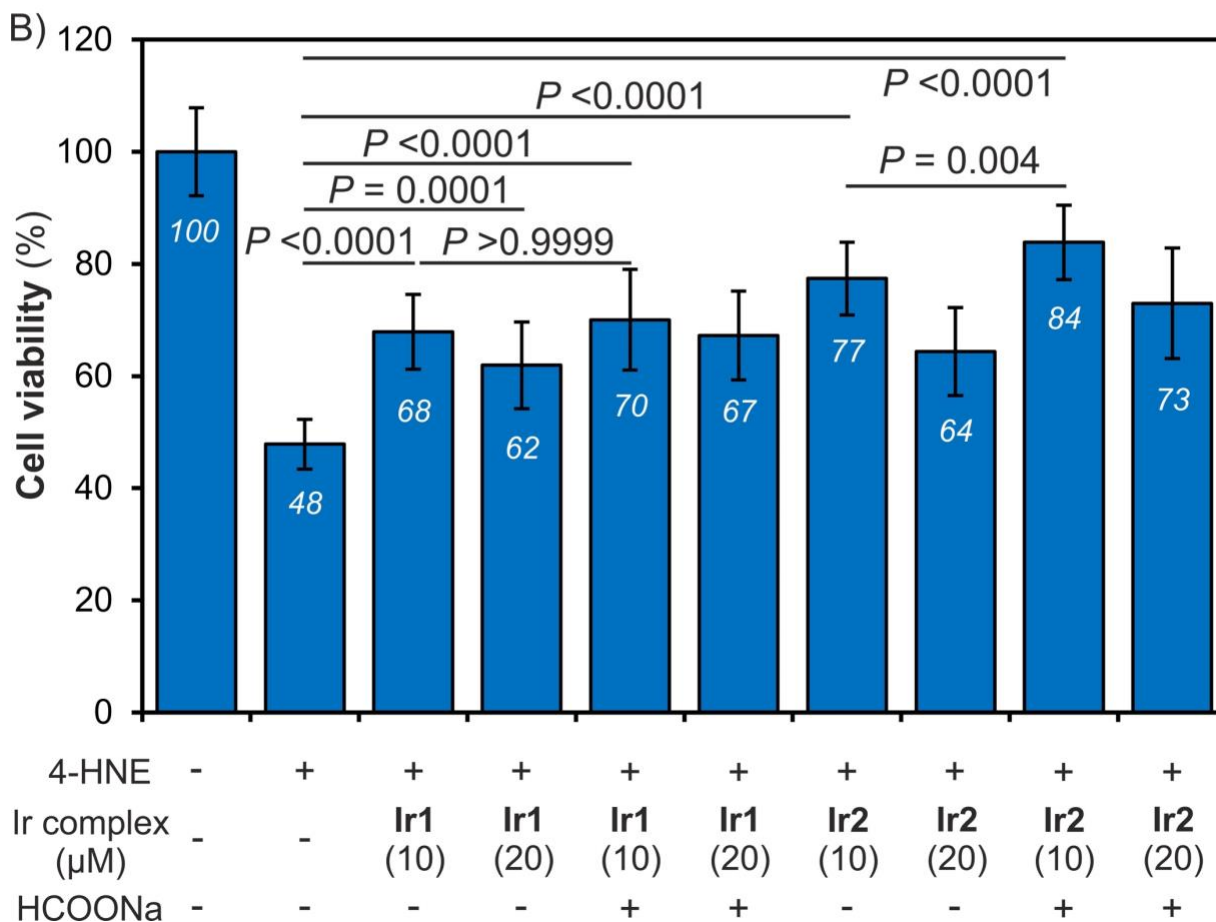
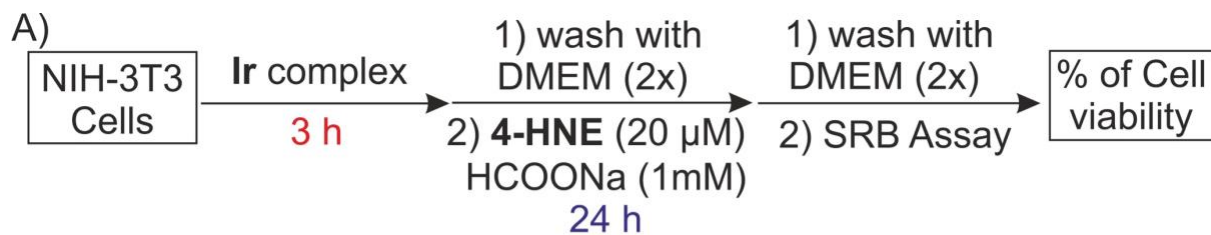


Figure S15. A) Experimental procedure for 4-HNE detoxification in NIH-3T3 cells. B) Effect of iridium complexes with or without HCOONa on NIH-3T3 cell viability in the presence of 4-HNE (20 μ M). Treatment conditions: Ir complex (10 or 20 μ M), 4-HNE (20 μ M), and HCOONa (1 mM). The data were analyzed using one-way ANOVA and shown as the mean \pm standard deviation ($n = 6$ per group).

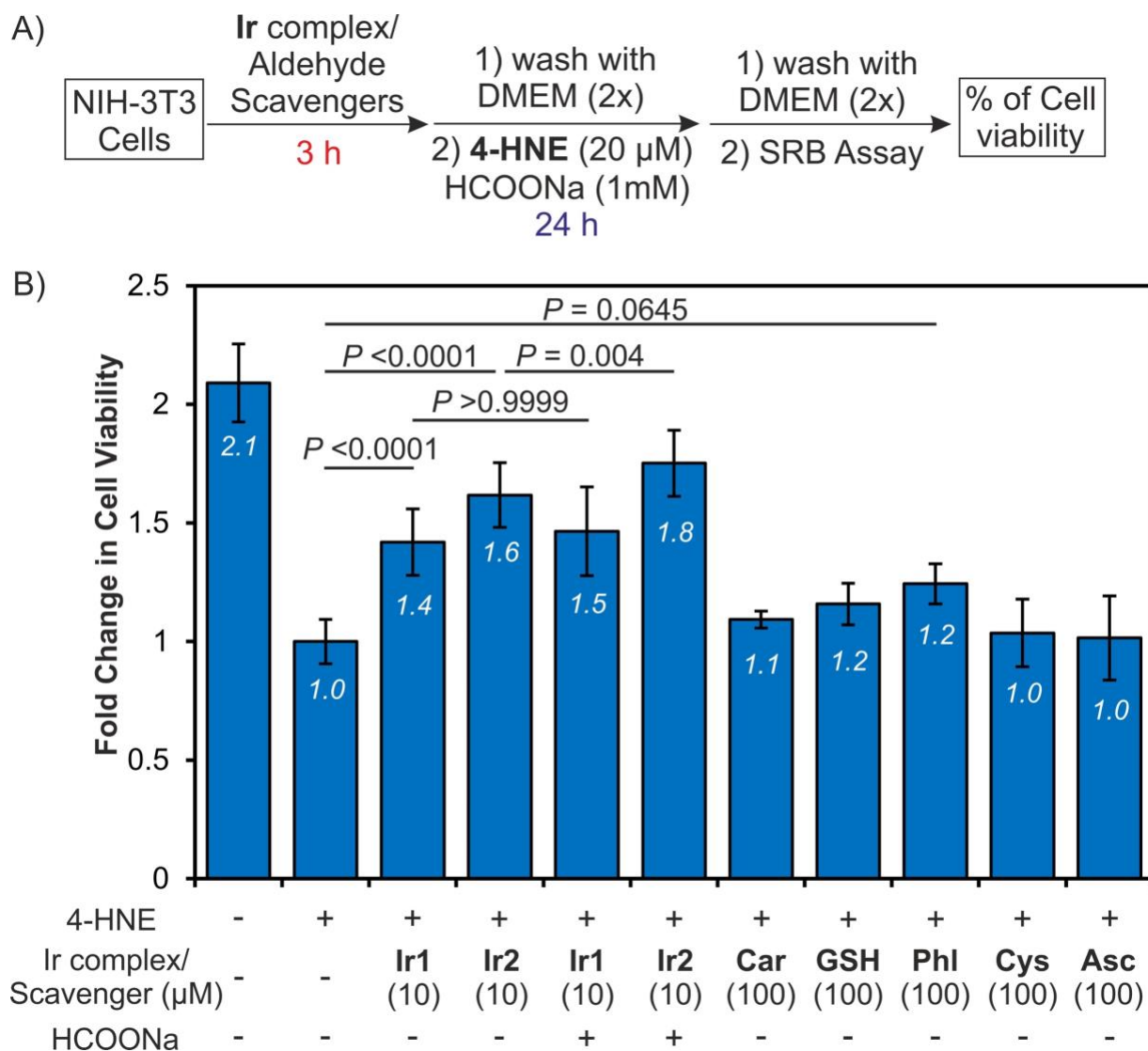


Figure S16. A) Experimental procedure for 4-HNE detoxification in NIH-3T3 cells. B) Comparison of the effects of the iridium complexes and aldehyde scavengers on the viability of NIH-3T3 cells after treatment with 4-HNE (20 μM). Treatment conditions: Ir complex (10 μM) or aldehyde scavengers (100 μM), and HCOONa (1mM). The fold change in cell viability was calculated as the ratio of the percentage of viable cells in treated wells divided by the percentage of viable cells in negative control wells containing only 4-HNE. The data were analyzed using one-way ANOVA and shown as the mean ± standard deviation ($n = 6$ per group). Abbreviations: Car = carnosine, GSH = reduced glutathione, Phl = phloretin, Cys = L-cysteine, Asc = sodium ascorbate.

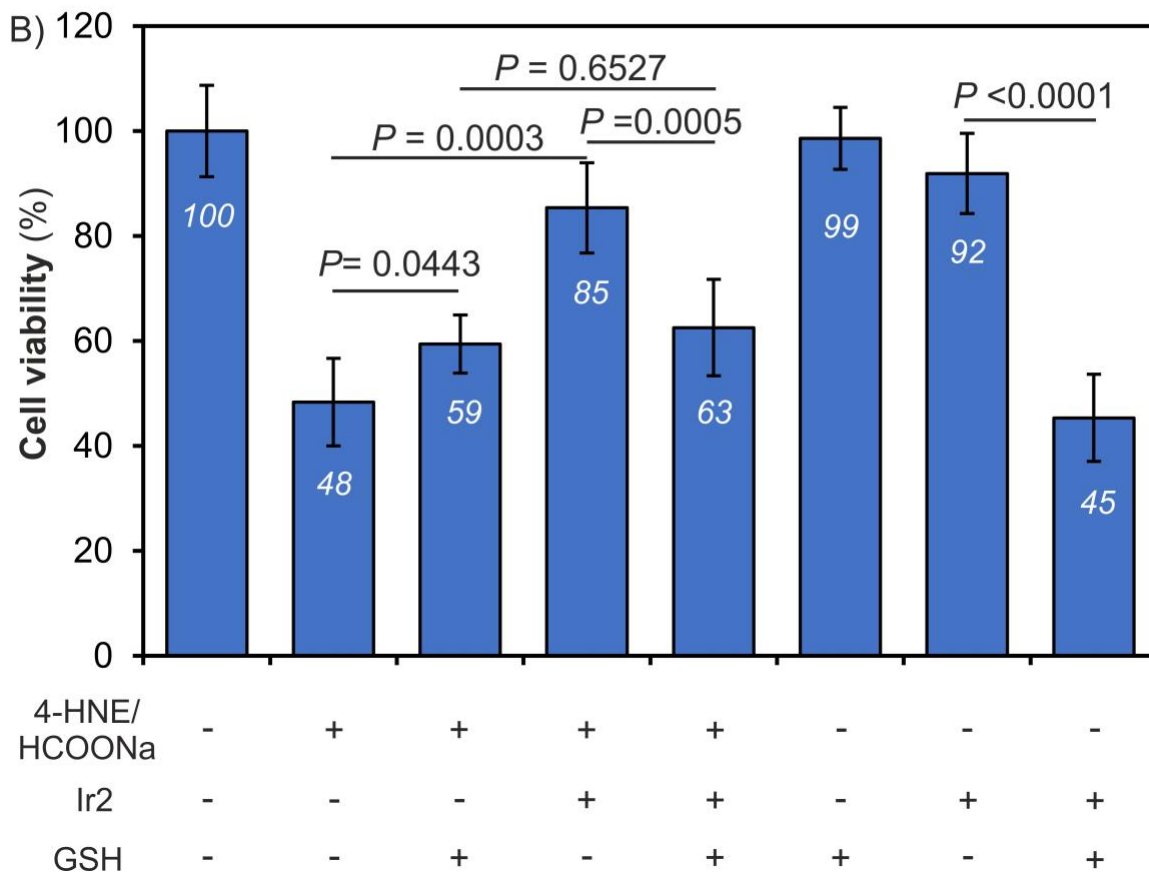
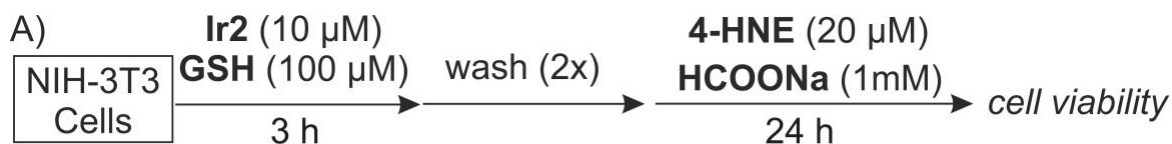


Figure S17. A) Experimental procedure for 4-HNE detoxification in NIH-3T3 cells with and without GSH. B) Comparison of the effects of the iridium complexes and Ir with and without GSH on the viability of NIH-3T3 cells after treatment with 4-HNE (20 μ M). Treatment conditions: Ir complex (10 μ M), GSH (100 μ M) and HCOONa (1mM). The fold change in cell viability was calculated as the ratio of the percentage of viable cells in treated wells divided by the percentage of viable cells in negative control wells containing only 4-HNE. The data were analyzed using one-way ANOVA and shown as the mean \pm standard deviation ($n = 6$ per group).

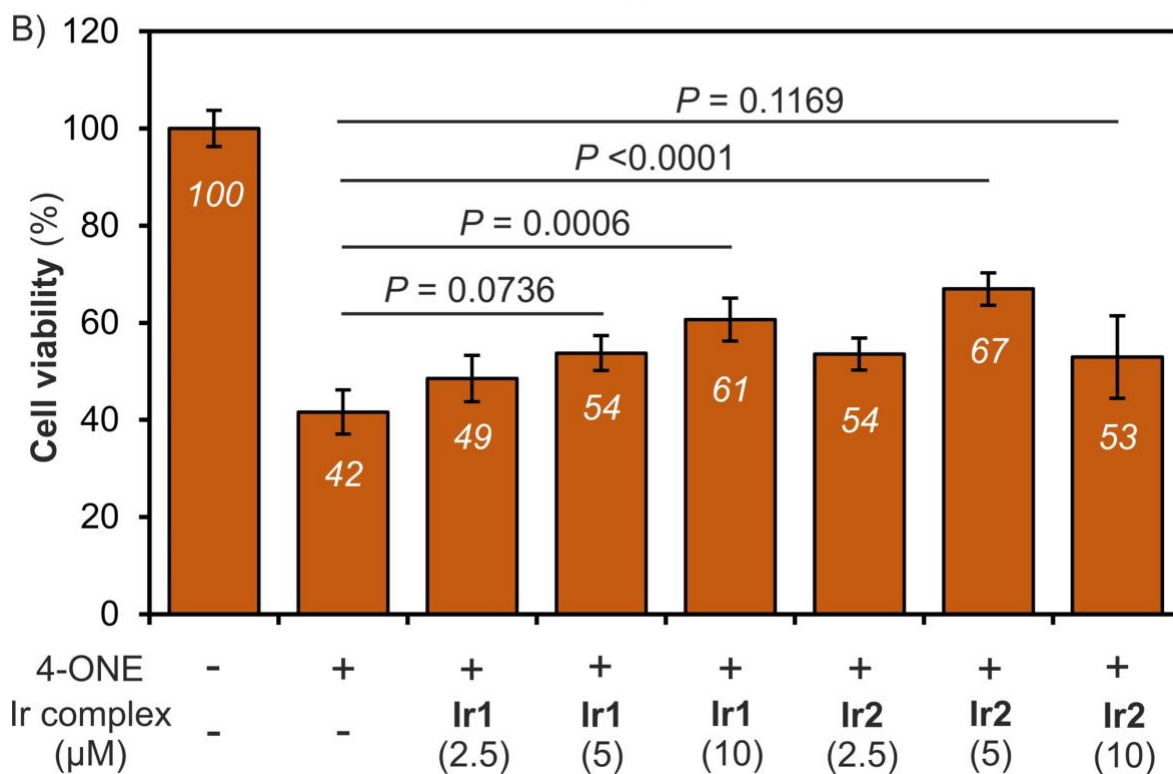
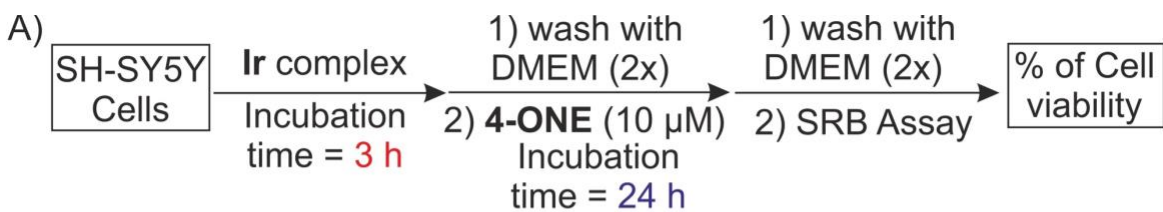


Figure S18. A) Experimental procedure for 4-ONE detoxification in SH-SY5Y cells. B) Effect of iridium complexes on SH-SY5Y cell viability in the presence of 4-ONE (10 μM). Treatment conditions: Ir complex (2.5, 5, or 10 μM), and 4-ONE (10 μM). The data were analyzed using one-way ANOVA and shown as the mean ± standard deviation ($n = 6$ per group).

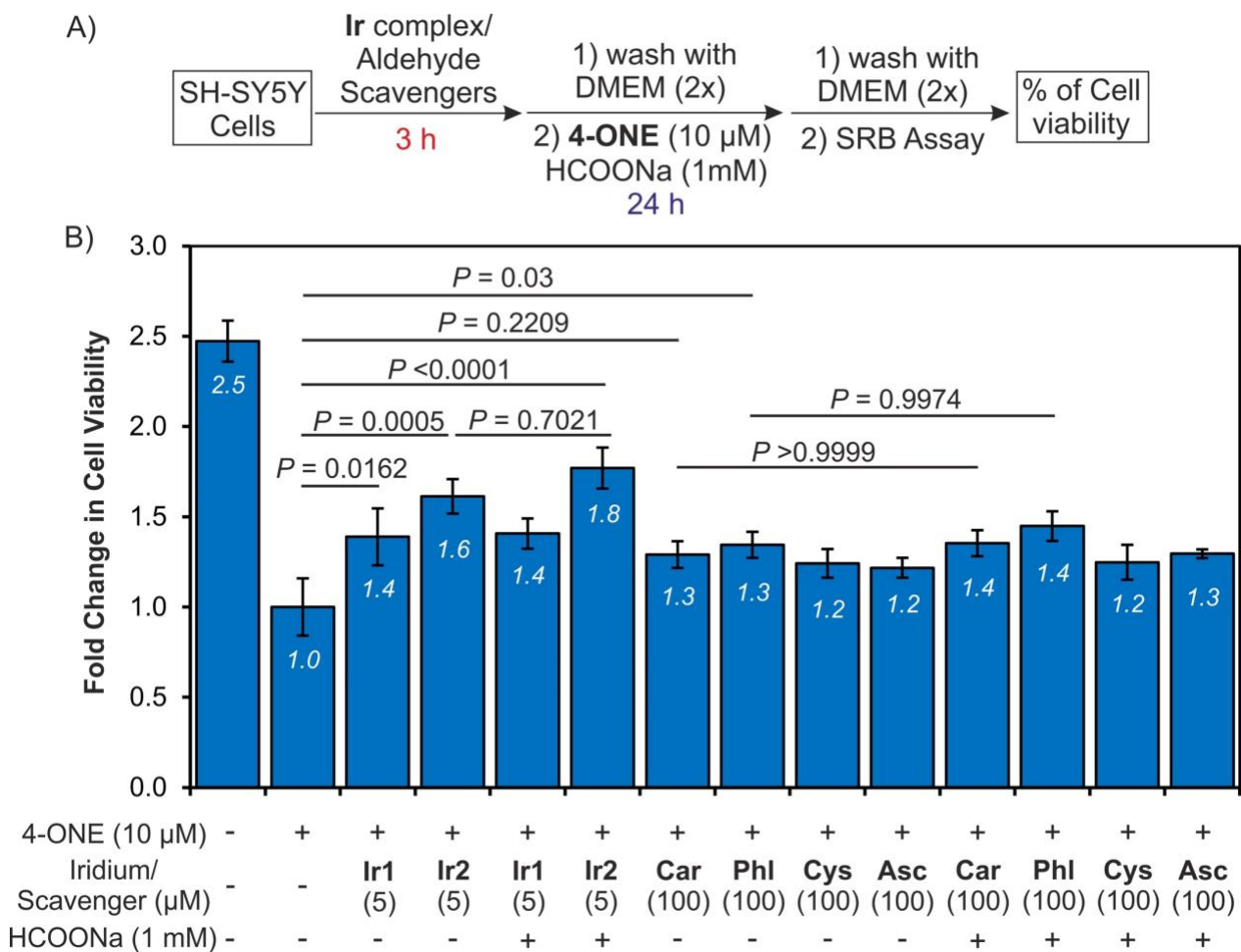


Figure S19. A) Experimental procedure for 4-ONE detoxification in SH-SY5Y cells. B) Comparison of the effects of iridium complexes and aldehyde scavengers on the viability of SH-SY5Y cells after exposure to 4-ONE (10 µM). Treatment conditions: Ir complex (5 µM), aldehyde scavengers (100 µM), and HCOONa (1 mM). The fold change in cell viability was calculated as the ratio of the viable cells % in treated wells divided by the viable cells % in negative control wells containing only 4-ONE. The data were analyzed using one-way ANOVA and shown as the mean \pm standard deviation ($n = 6$ per group). Abbreviations: Car = carnosine, GSH = reduced glutathione, Phl = phloretin, Cys = L-cysteine, Asc = sodium ascorbate.

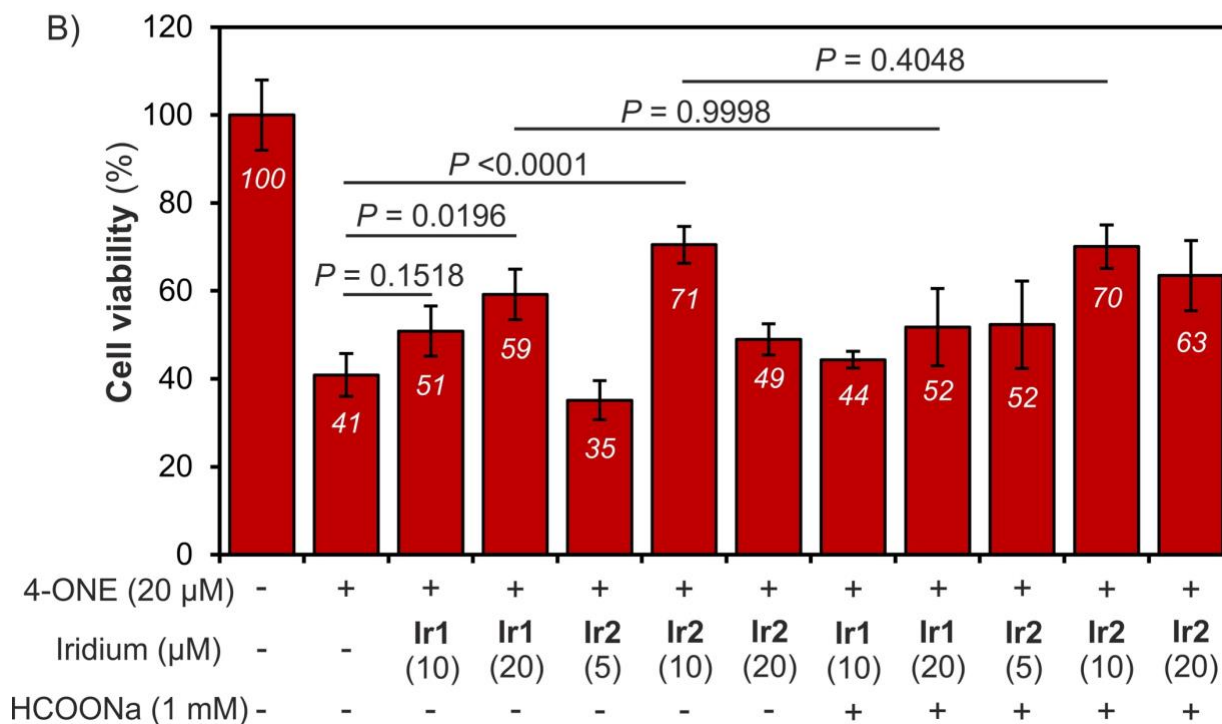
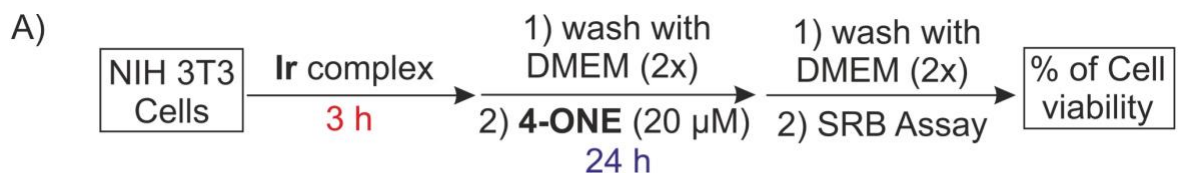


Figure S20. A) Experimental procedure for 4-ONE detoxification in NIH-3T3 cells. B) Effect of iridium complexes on NIH-3T3 cell viability in the presence of 4-ONE (20 μM). Treatment conditions: Ir complex (5, 10, or 20 μM), and HCOONa (1 mM). The fold change was calculated as the ratio of viable cells % in treated wells divided by the viable cells % in negative control wells containing only 4-ONE. The data were analyzed using one-way ANOVA and shown as the mean ± standard deviation ($n = 6$ per group).

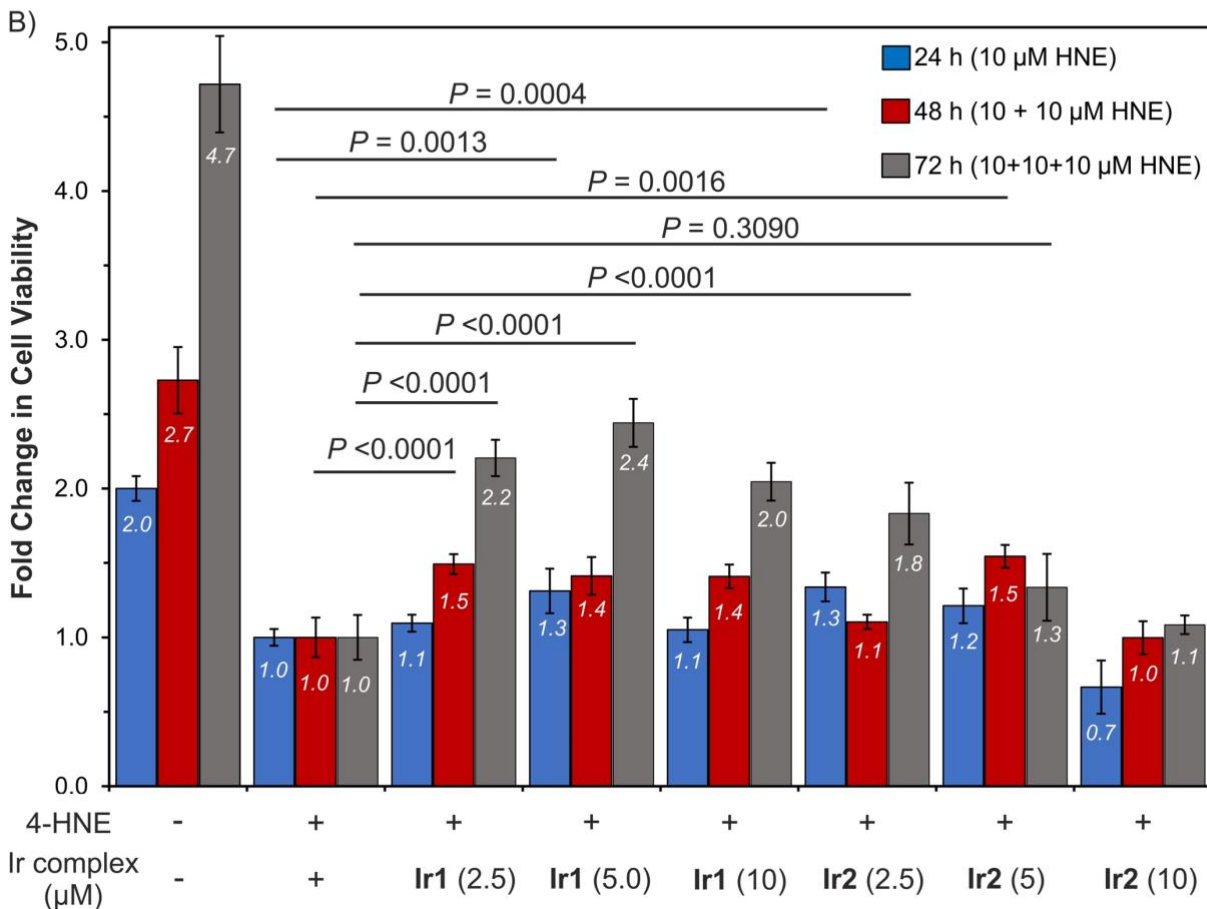
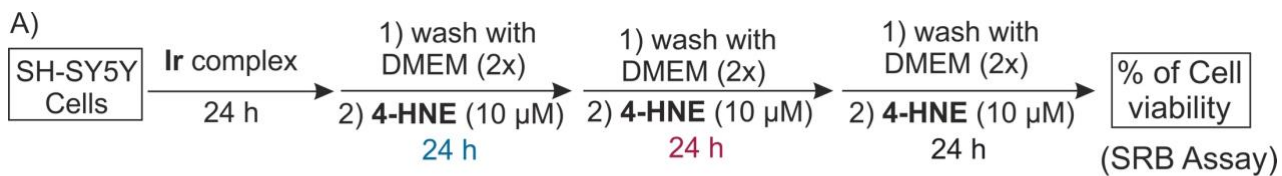


Figure S21. A) Experimental procedure for aldehyde detoxification after incubating SH-SY5Y cells with 4-HNE for three consecutive days. B) Effect of iridium complexes on SH-SY5Y cells after repeated exposure to 10 μM of 4-HNE. The fold change was measured after 24 h (blue), 48 h (red), and 72 h (gray). The fold change was calculated as the ratio of viable cells % in treated wells divided by the viable cells % in negative control wells containing only 4-HNE. The data were analyzed using one-way ANOVA and shown as the mean ± standard deviation ($n = 6$ per group).

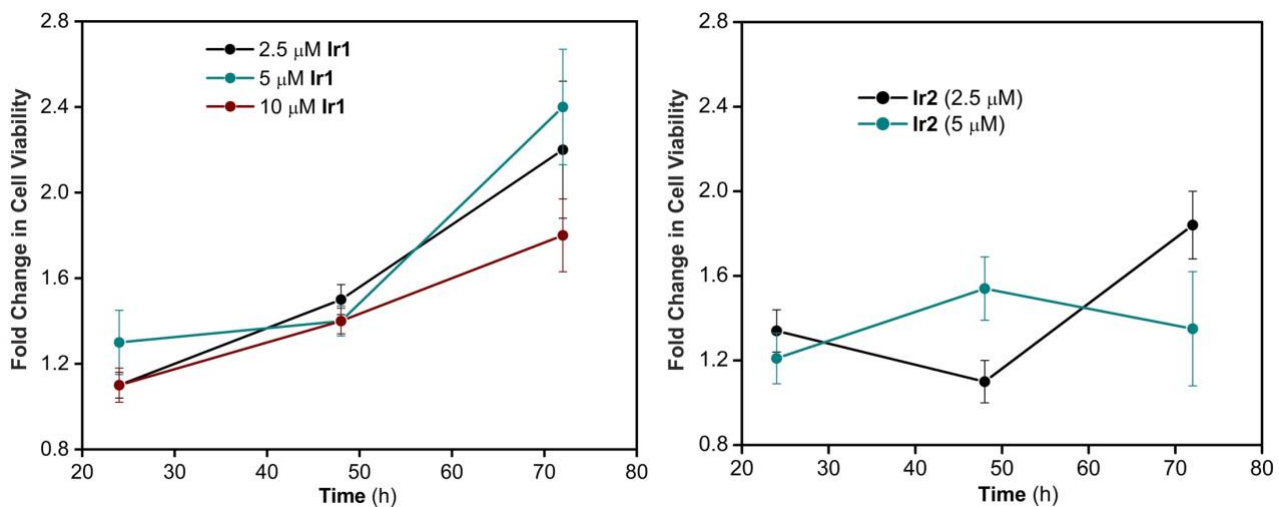


Figure S22. Comparing the ability of the iridium complexes to protect SH-SY5Y cells against repeated exposure to 4-HNE. It was observed that cells treated with lower concentrations of Ir exhibited greater viability after 72 h compared to those treated with higher concentrations. The data are shown as the mean \pm standard deviation ($n = 6$ per group).

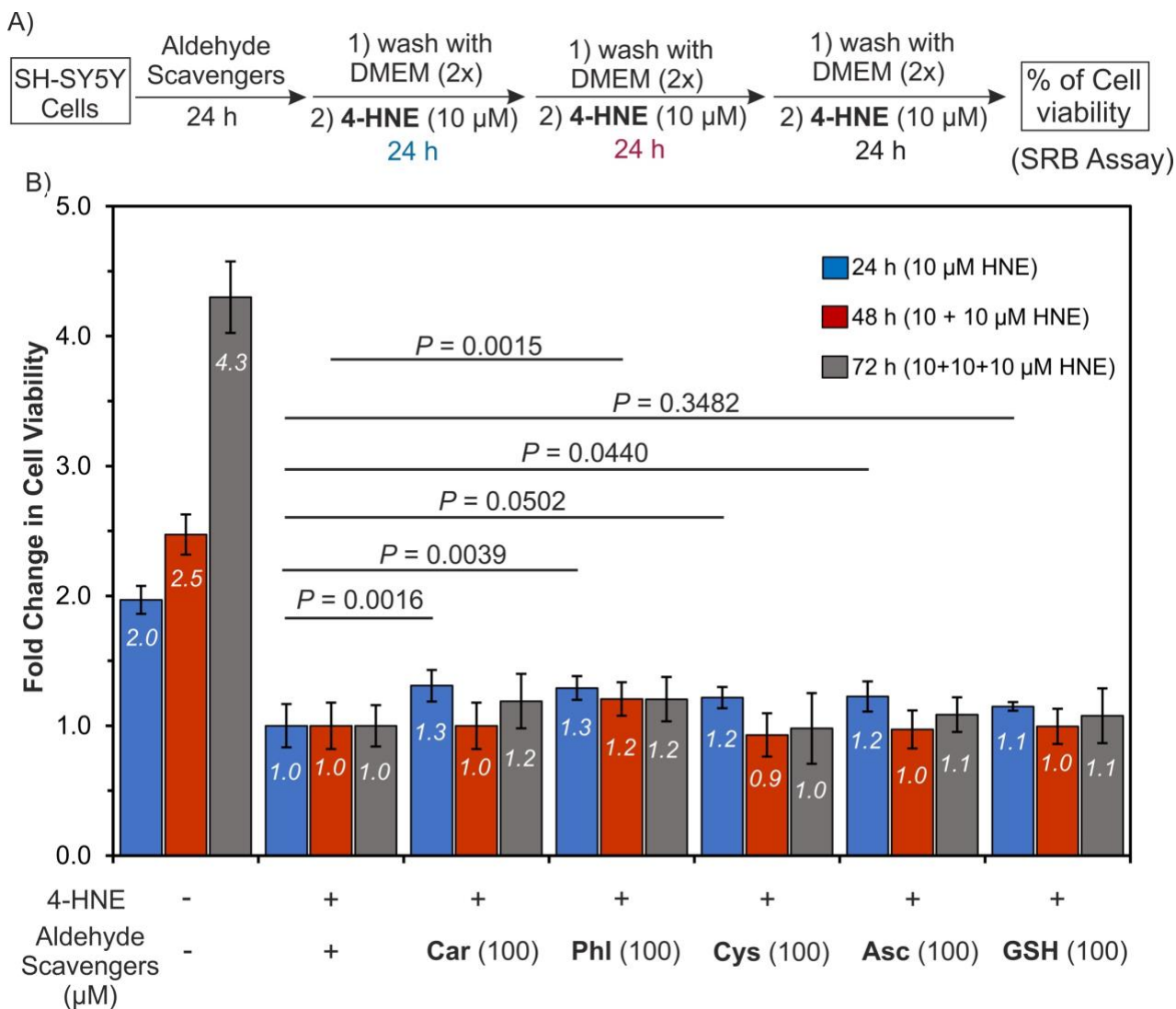


Figure S23. A) Experimental procedure for aldehyde detoxification after incubating SH-SY5Y cells with 4-HNE for three consecutive days. B) Effect of aldehyde scavengers (100 µM) on SH-SY5Y cells after repeated exposure to 10 µM of 4-HNE. The fold change was measured after 24 h (blue), 48 h (red), and 72 h (gray). The fold change was calculated as the ratio of viable cells % in treated wells divided by the viable cells % in negative control wells containing only 4-HNE. The data were analyzed using one-way ANOVA and shown as the mean \pm standard deviation ($n = 6$ per group). Abbreviations: Car = carnosine, GSH = reduced glutathione, Phl = phloretin, Cys = L-cysteine, Asc = sodium ascorbate.

Characterization Data

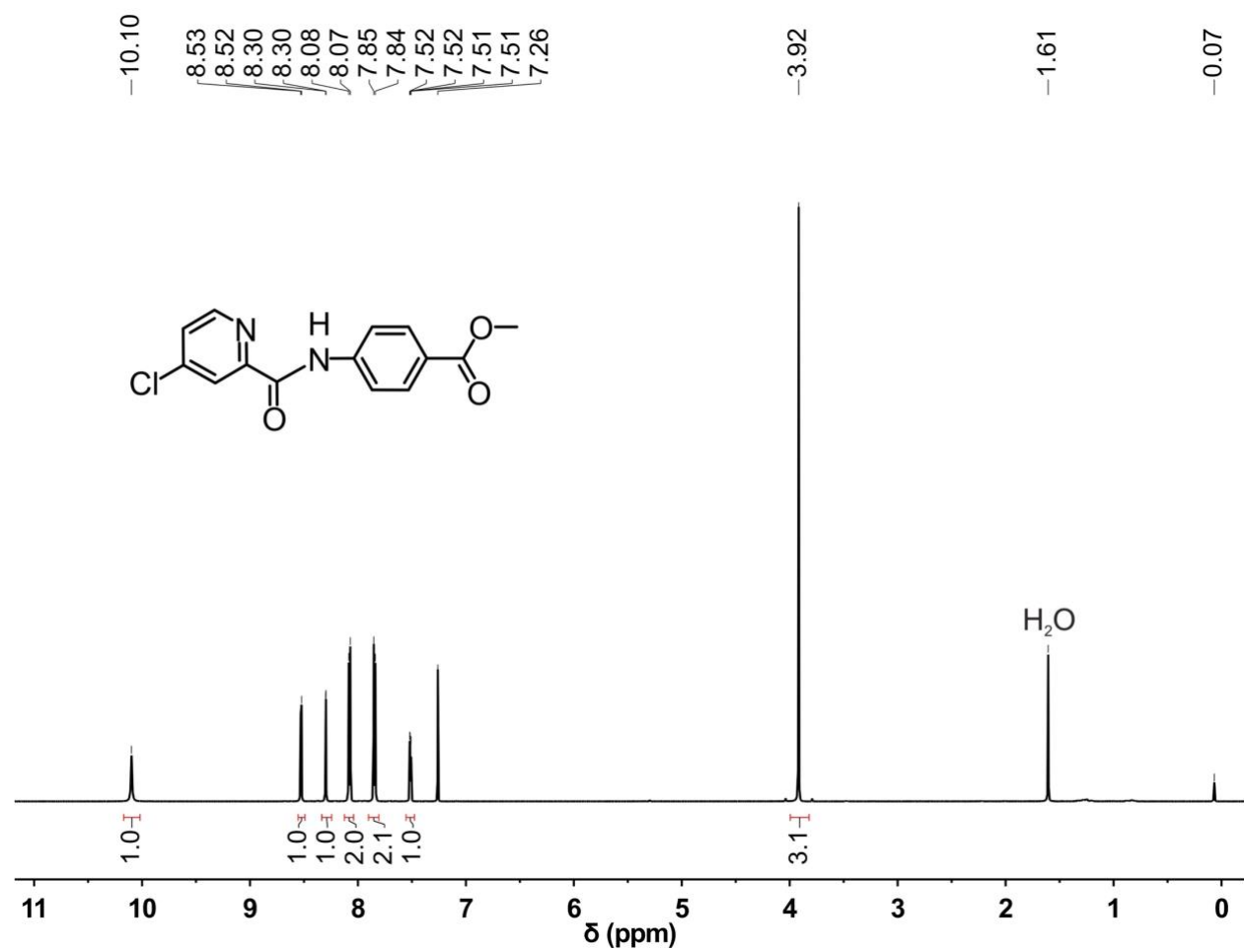


Figure S24. ¹H NMR spectrum (CDCl₃, 600 MHz) of 1.

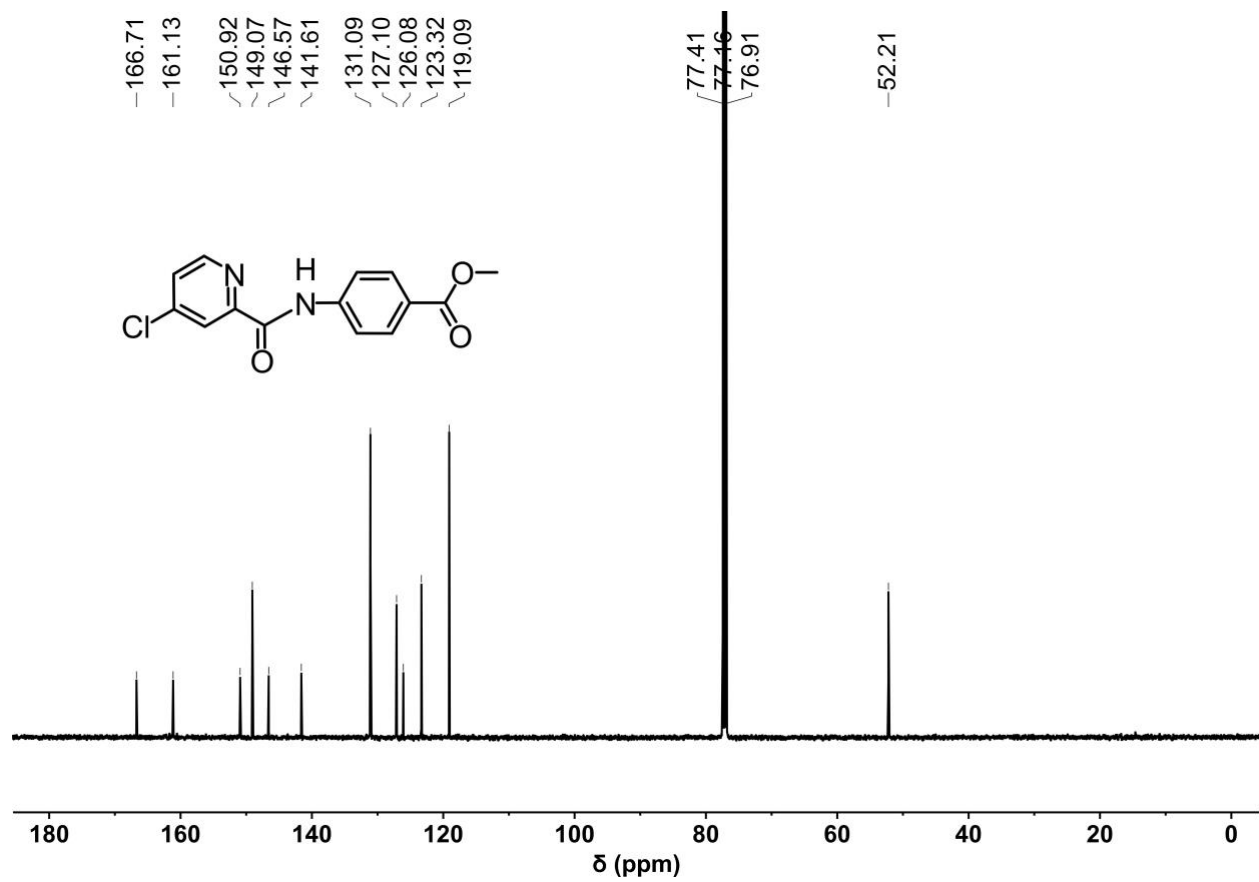


Figure S25. ¹³C NMR spectrum (CDCl₃, 126 MHz) of 1.

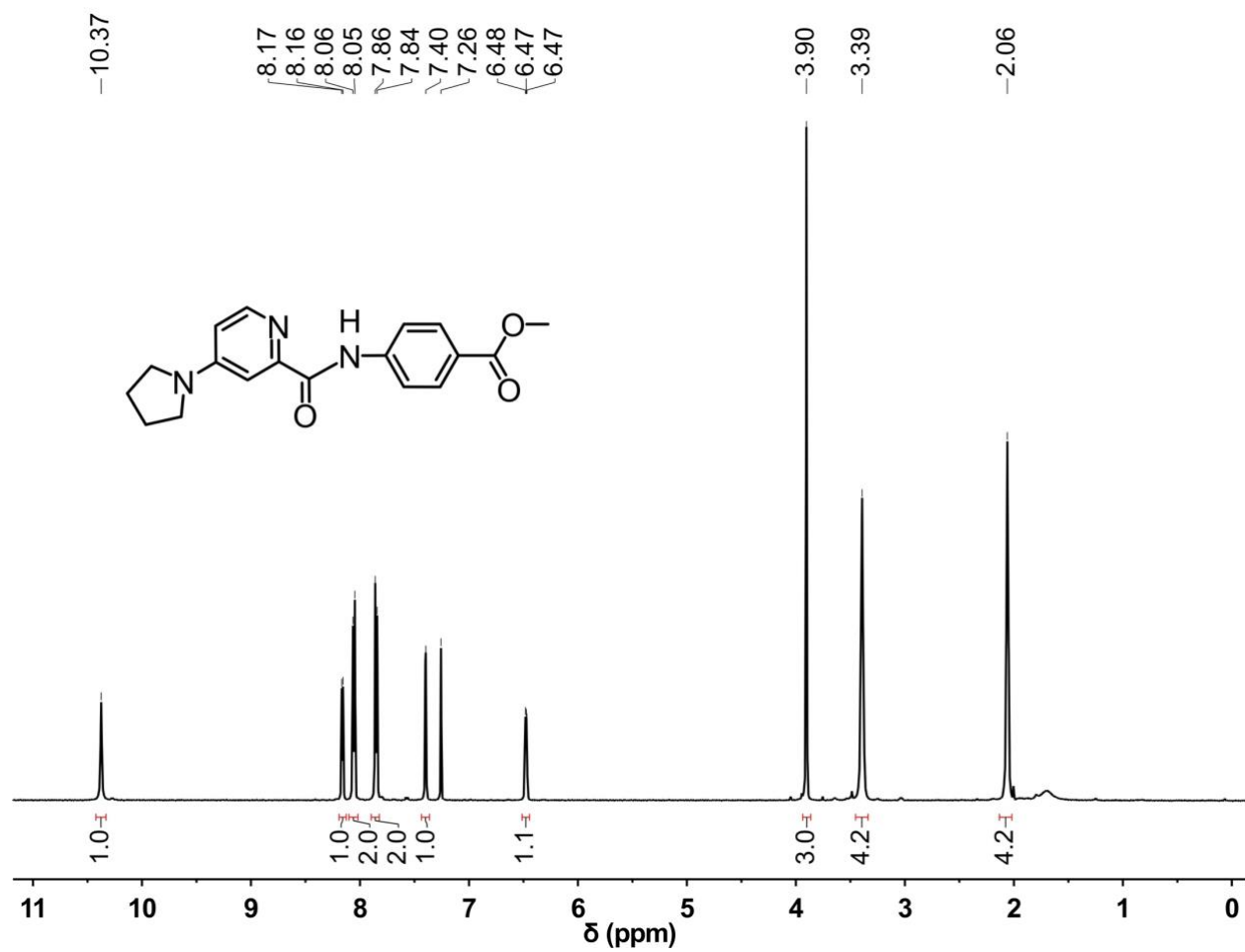


Figure S26. ¹H NMR spectrum (CDCl₃, 600 MHz) of L2.

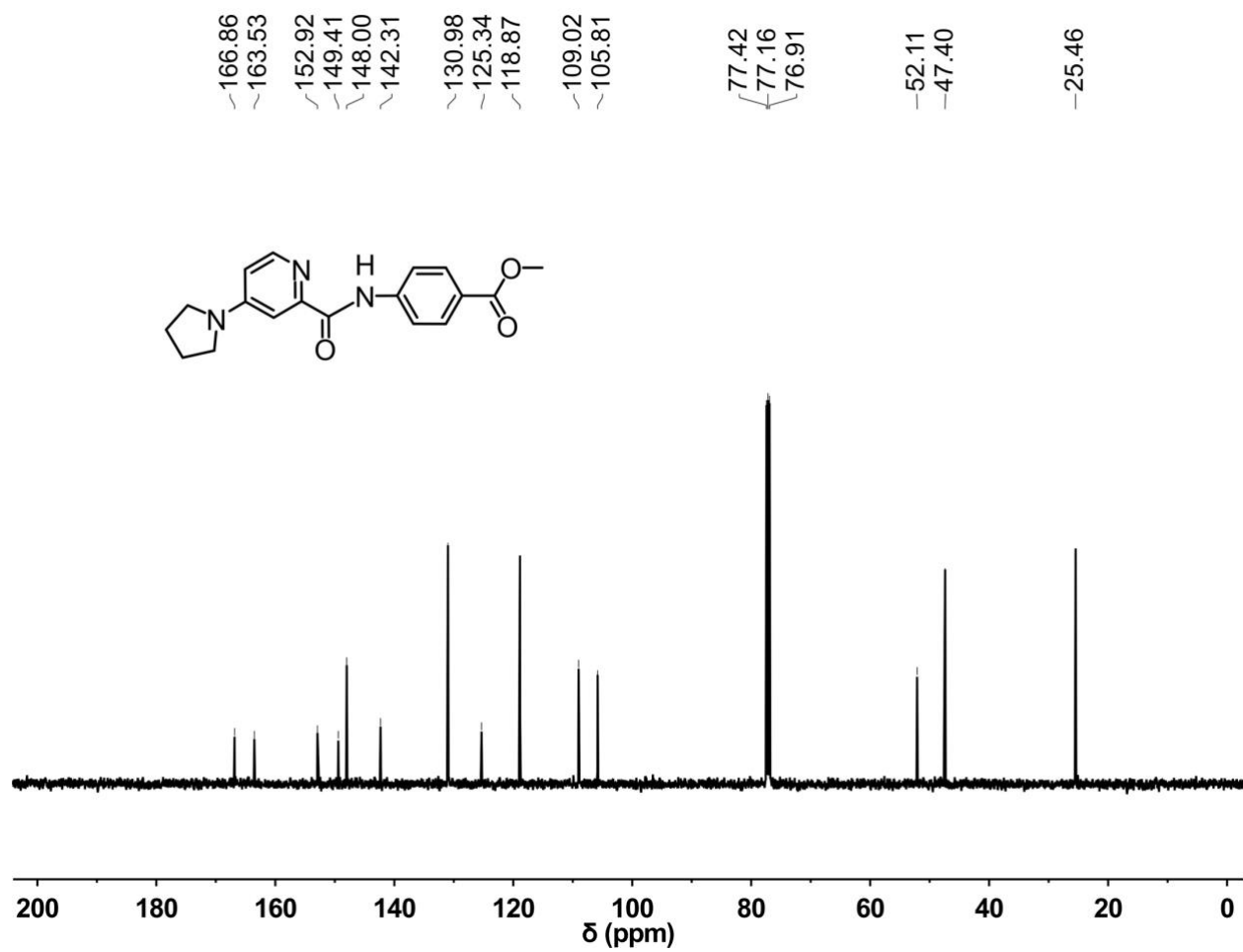


Figure S27. ^{13}C NMR spectrum (CDCl₃, 126 MHz) of L2.

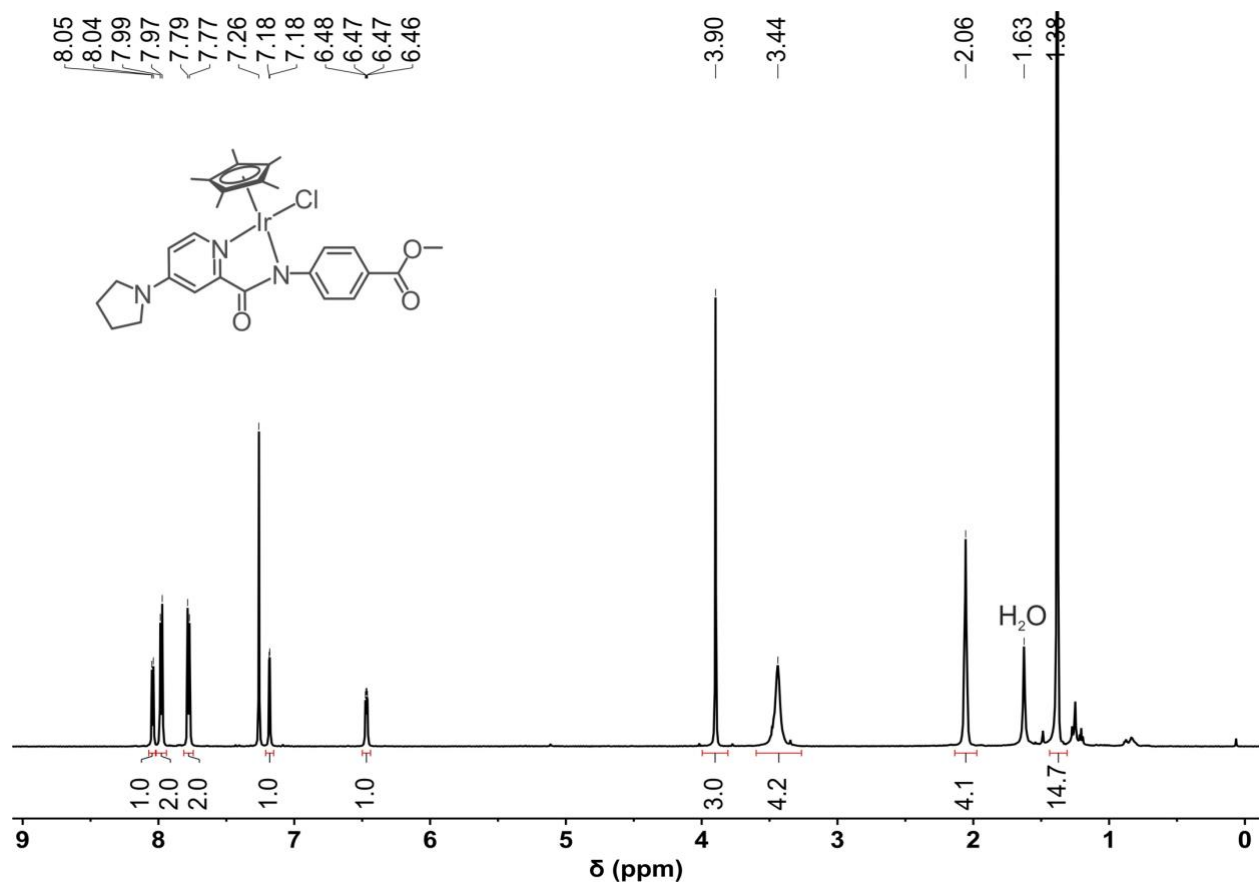


Figure S28. ¹H NMR spectrum (CDCl₃, 400 MHz) of Ir2.

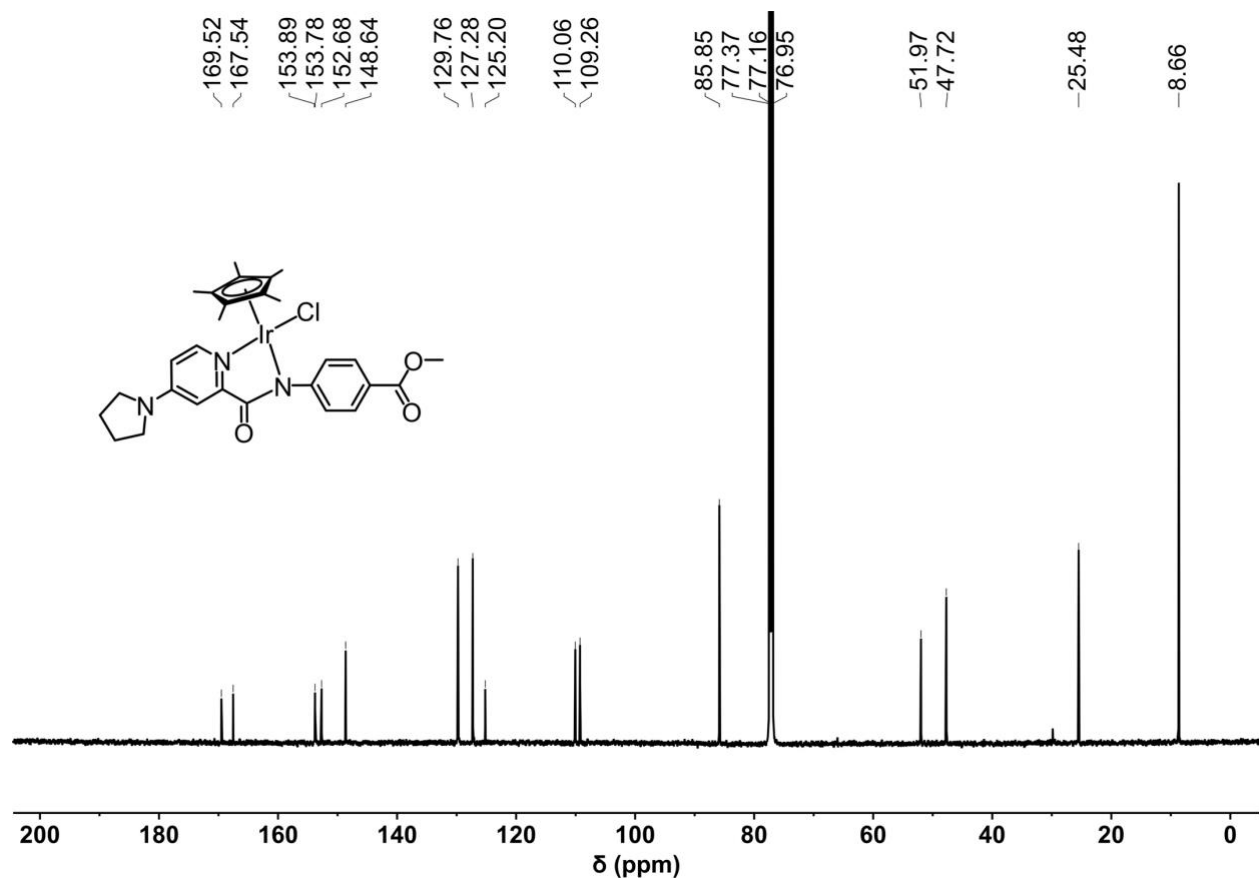


Figure S29. ¹³C NMR spectrum (CDCl₃, 151 MHz) of Ir2.

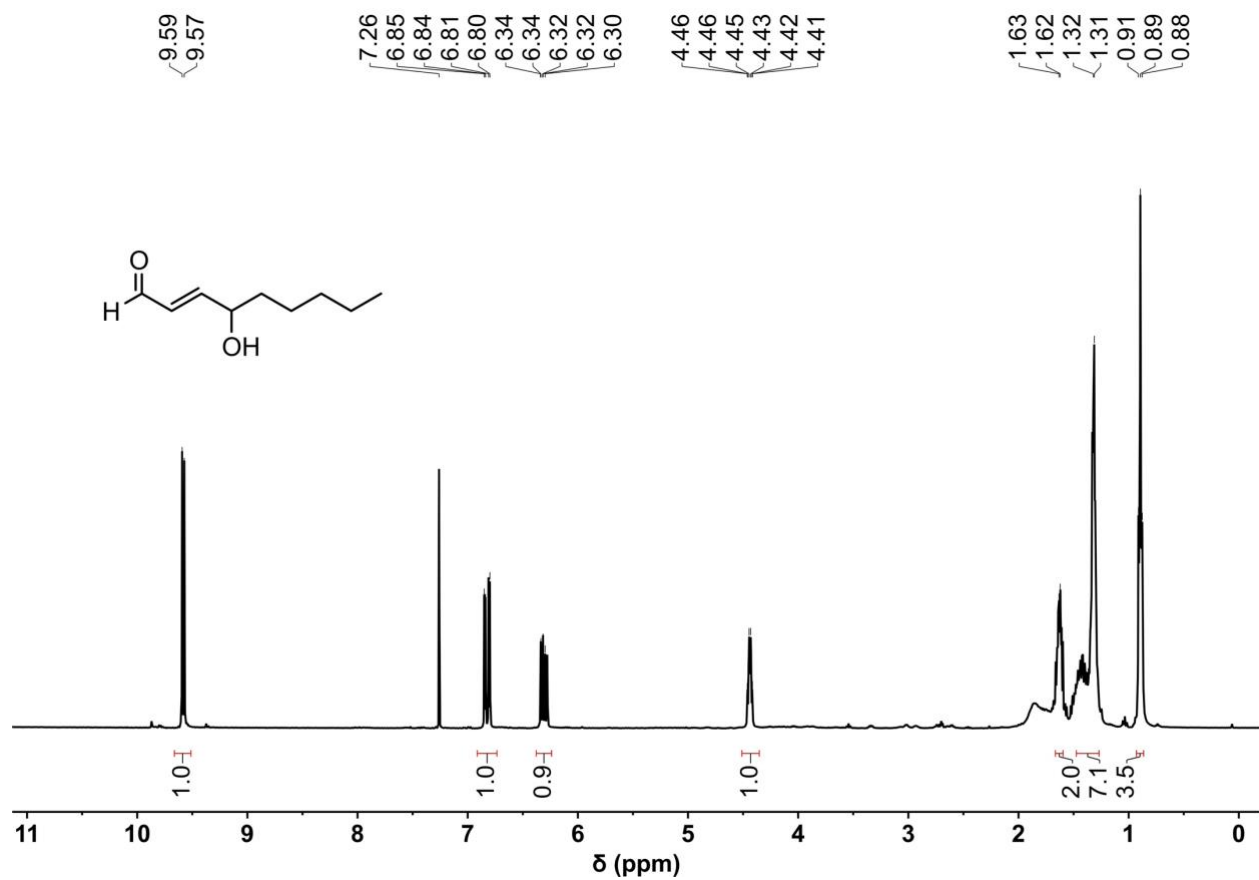


Figure S30. ^1H NMR spectrum (CDCl₃, 400 MHz) of 4-HNE.

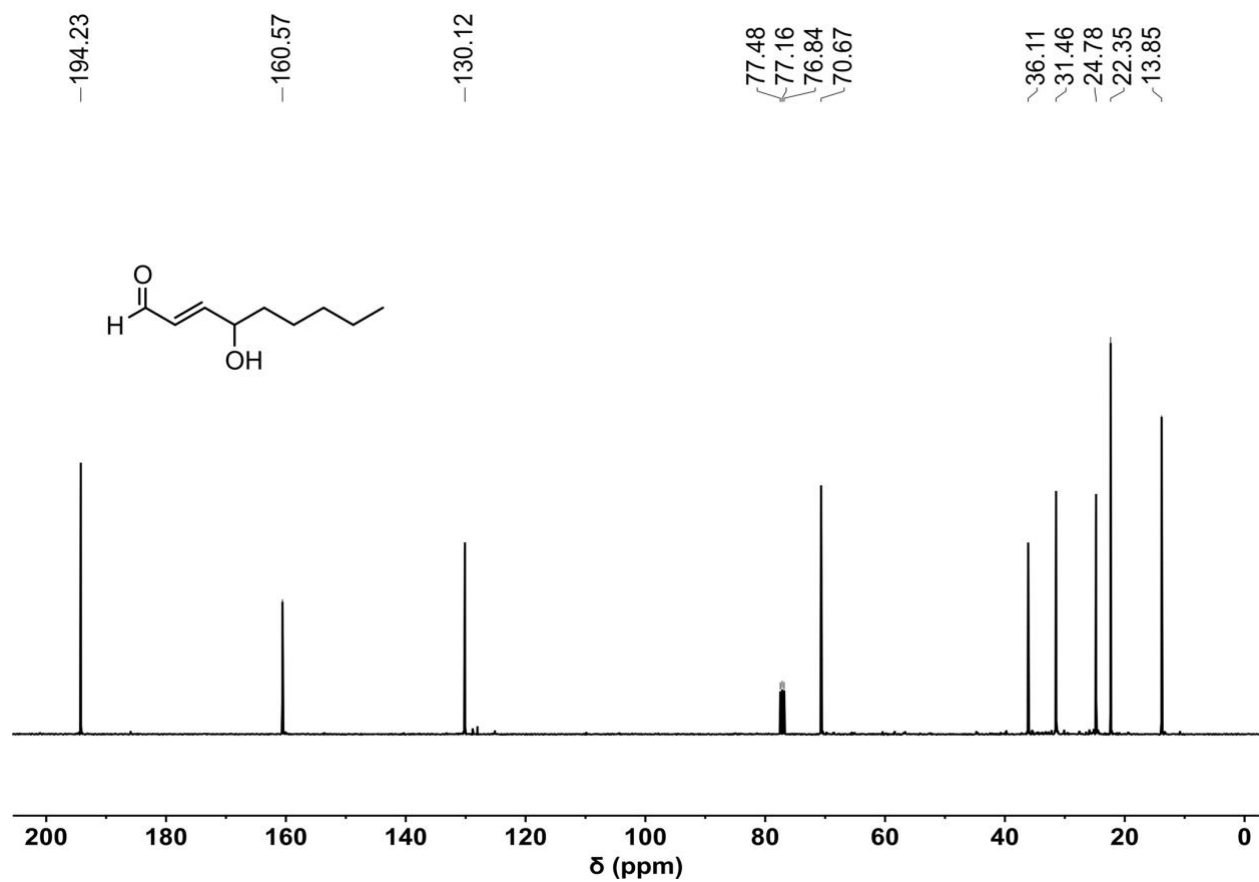


Figure S31. ¹³C NMR spectrum (CDCl₃, 101 MHz) of 4-HNE.

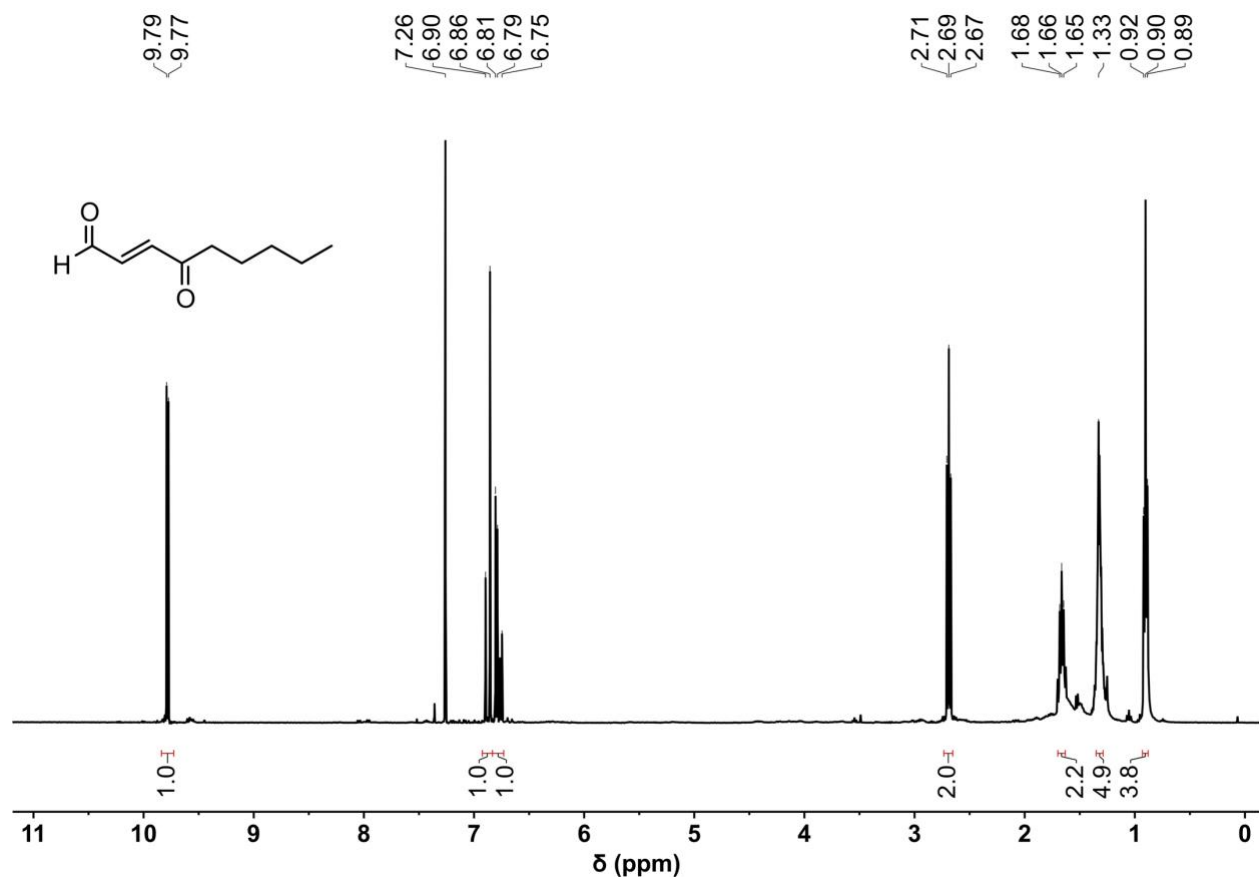


Figure S32. ^1H NMR spectrum (CDCl_3 , 400 MHz) of 4-ONE.

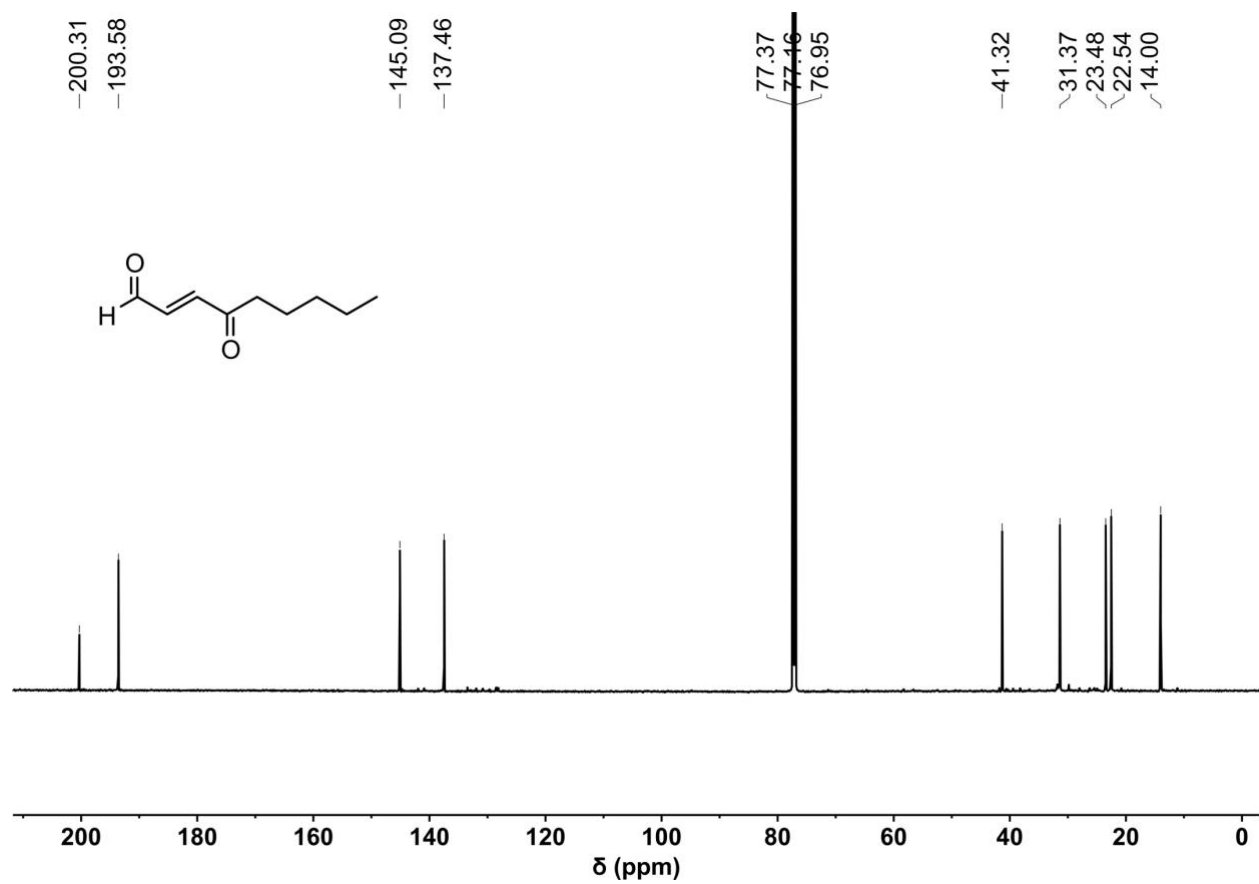


Figure S33. ¹³C NMR spectrum (CDCl₃, 151 MHz) of 4-ONE.

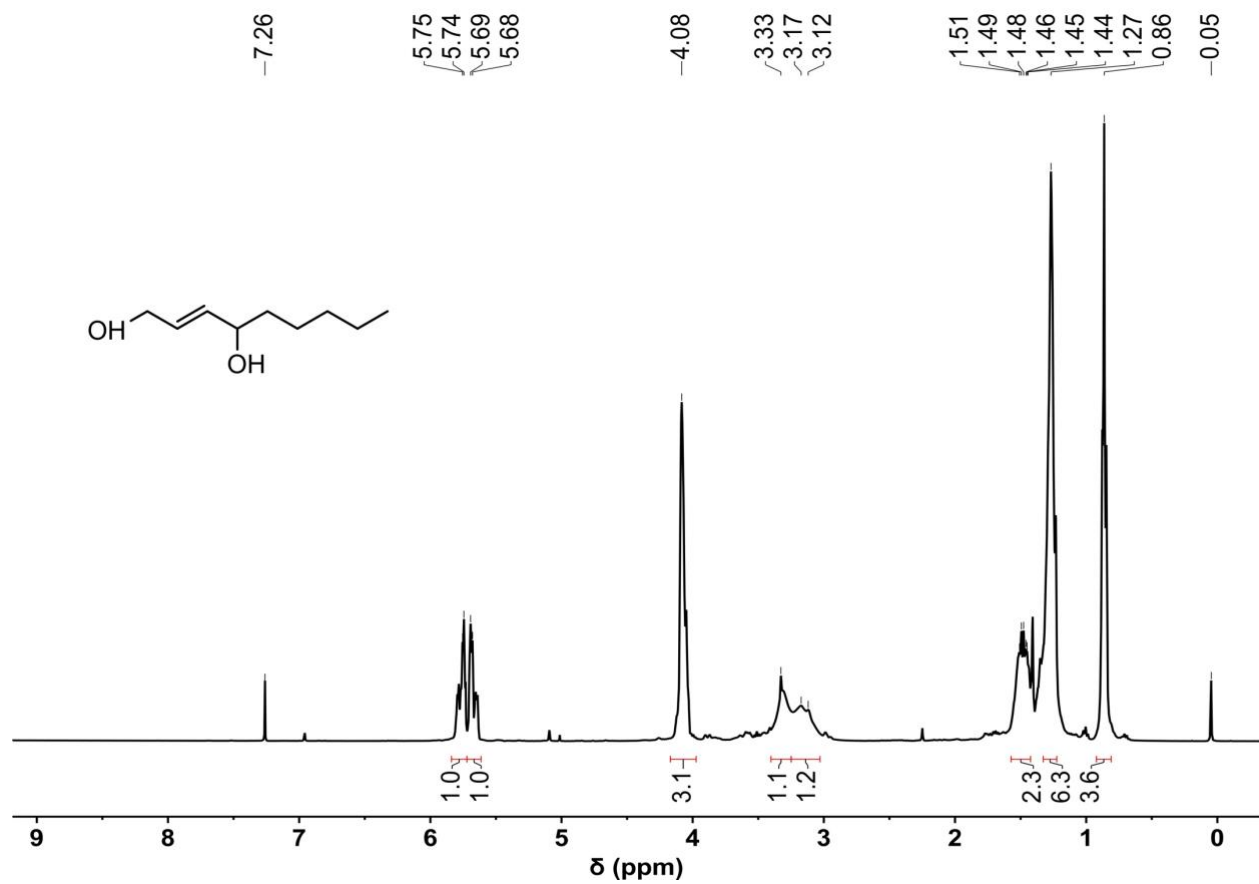


Figure S34. ¹H NMR spectrum (CDCl₃, 400 MHz) of compound I.

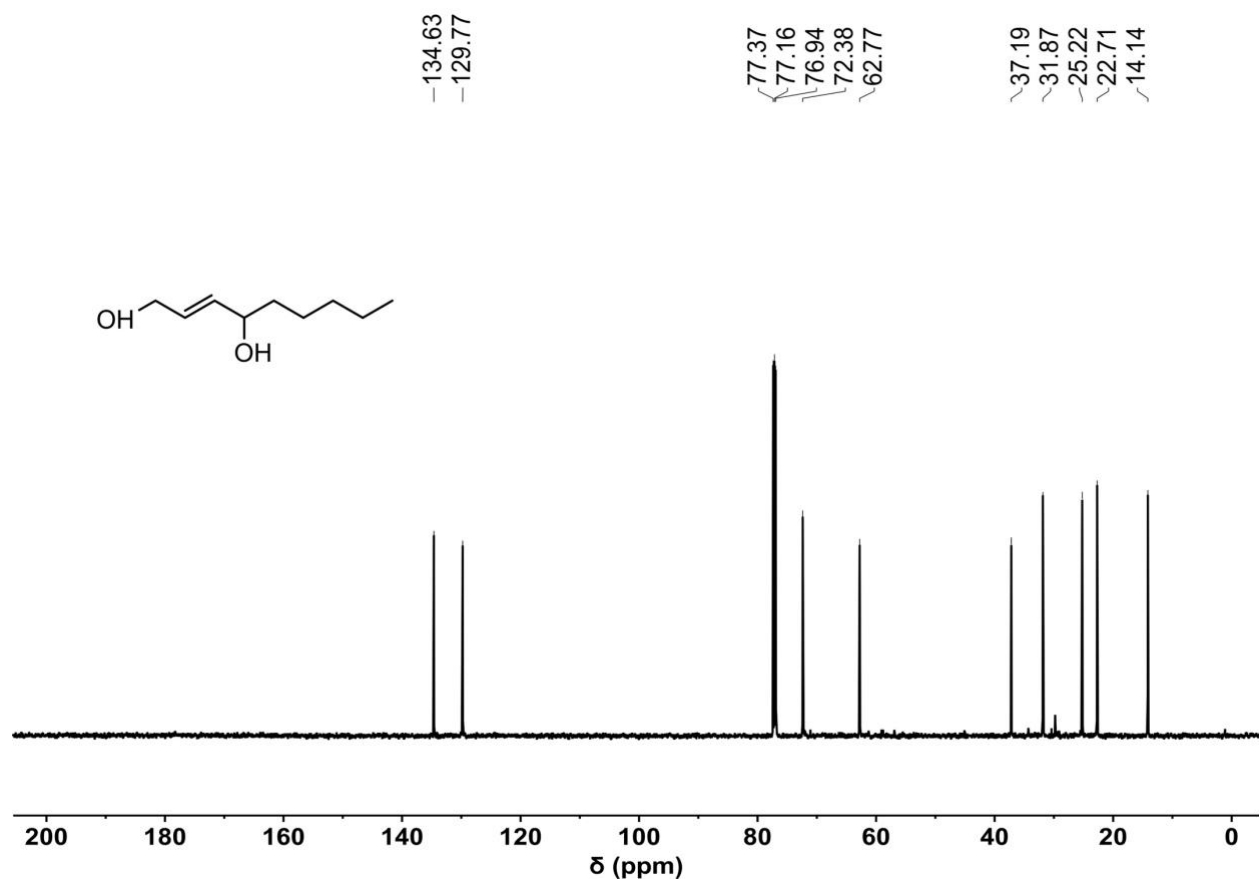


Figure S35. ^{13}C NMR spectrum (CDCl₃, 151 MHz) of compound I.

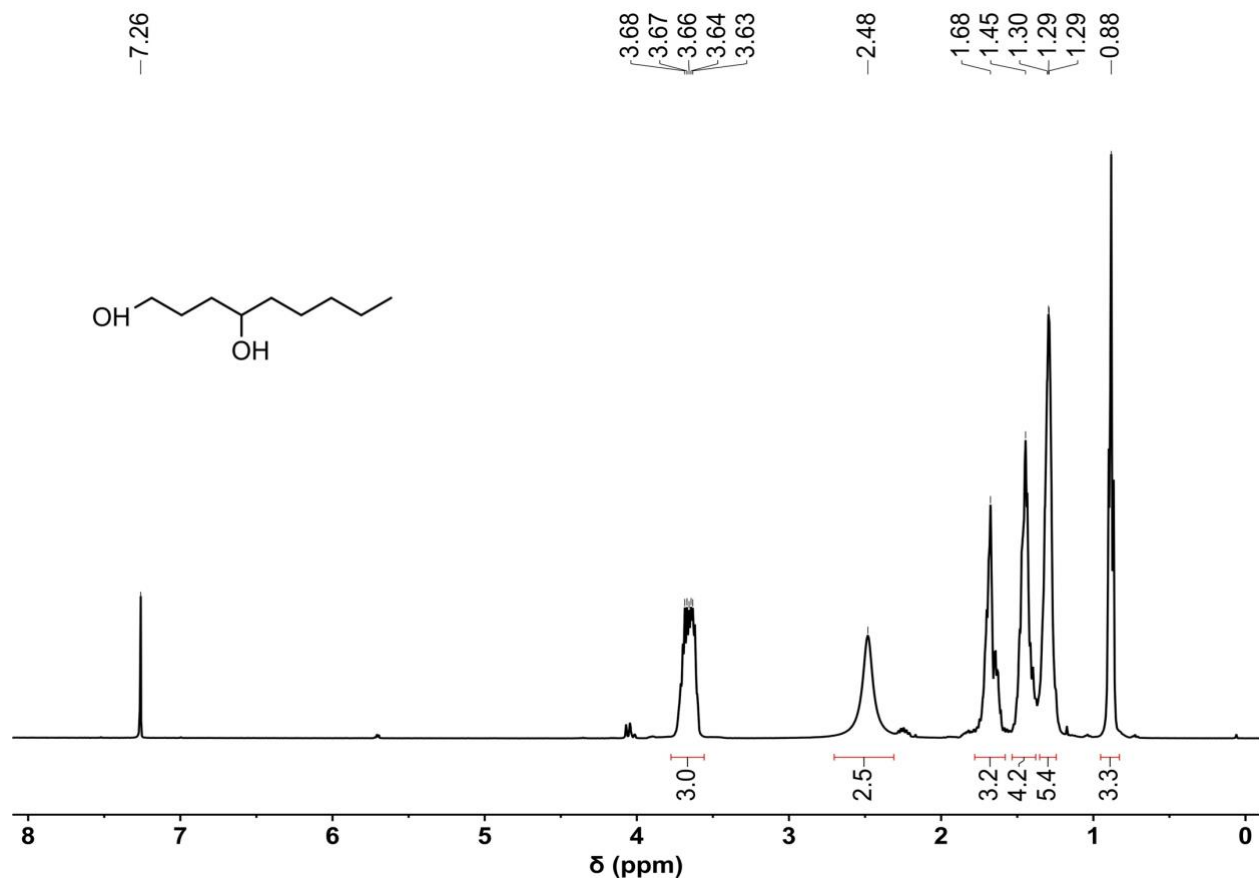


Figure S36. ¹H NMR spectrum (CDCl₃, 500 MHz) of compound II.

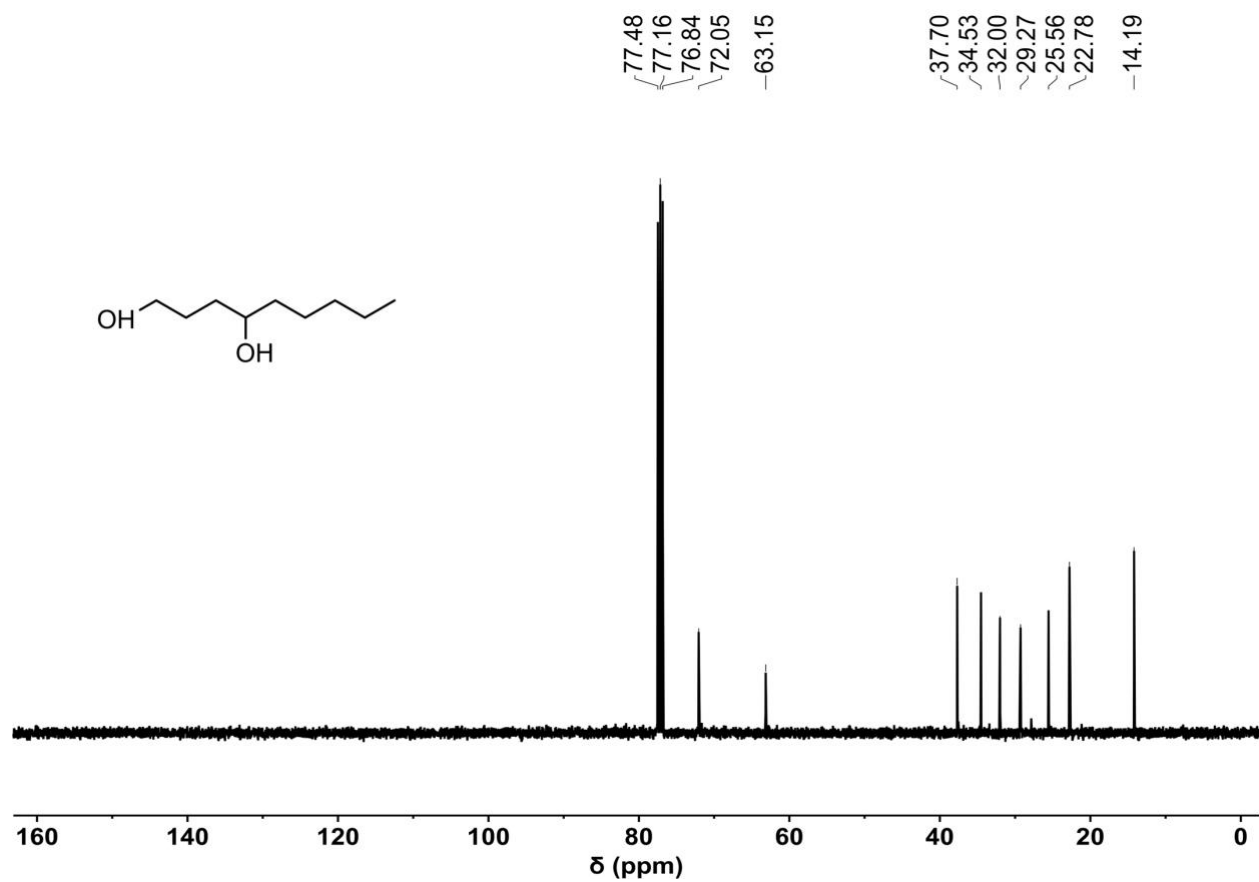


Figure S37. ^{13}C NMR spectrum (CDCl₃, 101 MHz) of compound II.

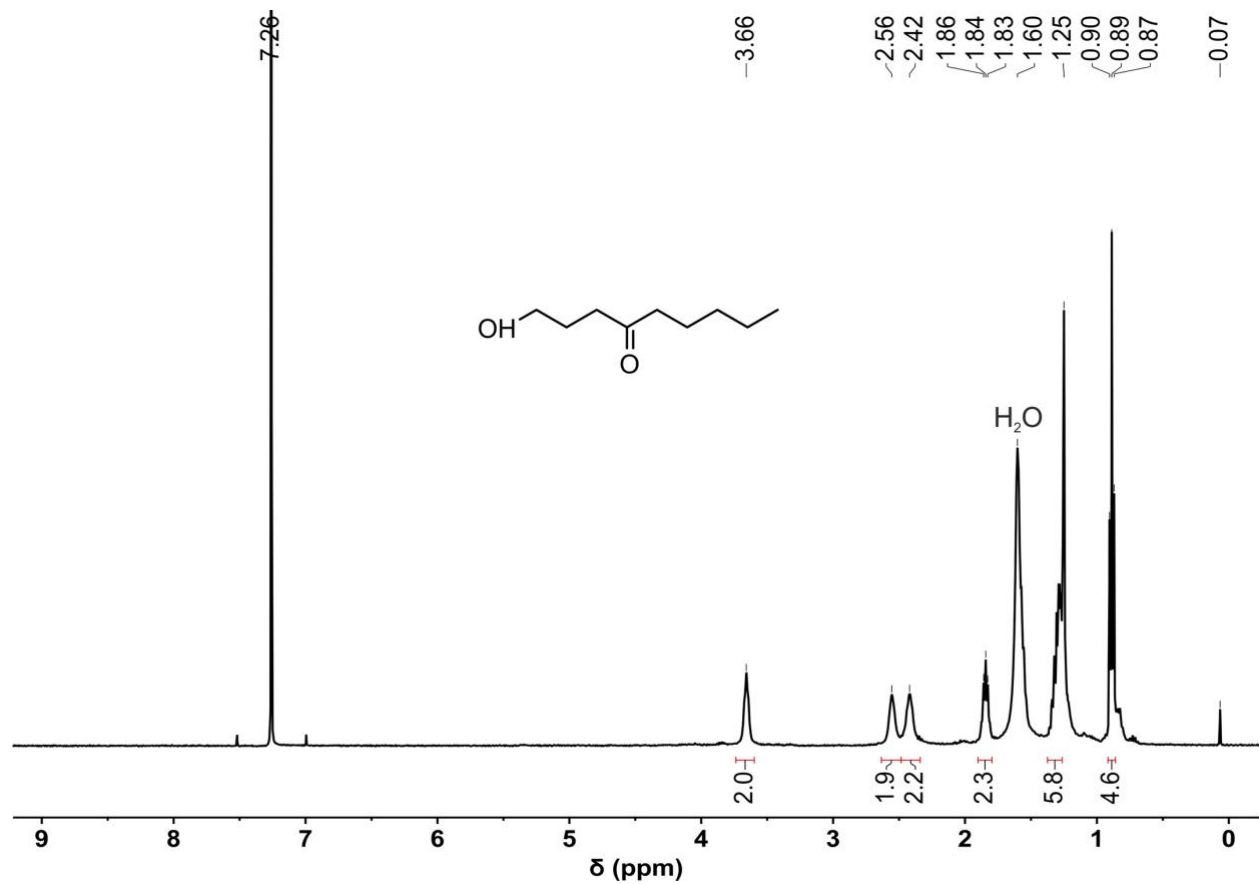


Figure S38. ¹³C NMR spectrum (CDCl₃, 500 MHz) of compound III.

References

- (1) Gardner, H. W.; Bartelt, R. J.; Weisleder, D. *Lipids* **1992**, *27*, 686-689.
- (2) McGrath, C. E.; Tallman, K. A.; Porter, N. A.; Marnett, L. J. *Chem. Res. Toxicol.* **2011**, *24*, 357-370.
- (3) Bates, R. W.; Díez-Martín, D.; Kerr, W. J.; Knight, J. G.; Ley, S. V.; Sakellaridis, A. *Tetrahedron* **1990**, *46*, 4063-4082.
- (4) Guo, J.; Wang, H.; Hrinczenko, B.; Salomon, R. G. *Chem. Res. Toxicol.* **2016**, *29*, 1187-1197.
- (5) Fuji, K.; Usami, Y.; Kiryu, Y.; Node, M. *Synthesis* **1992**, *1992*, 852-858.